Heavy Quark Physics
Grant No. DE-FG-01-ER-45863

Final Report

to the

Department of Energy
Office of Science

December 2003

Angel M. Lopez

University of Puerto Rico
Mayaguez, Puerto Rico

DISCLAIMER

Contents

Chapter 1

Project Description

1.1 Introduction and Overview

This project was carried out by personnel from the High Energy Physics Group at the University of Puerto Rico's Recinto Universitario de Mayaguez (Mayaguez Campus - UPR/RUM) which has been an active participant in experiments at Fermi National Accelerator Laboratory (Fermilab)(Batavia, Illinois) since 1985. The project consisted of participation in two experiments at Fermilab to study the behavior of two heavy quarks, charm and bottom.

The first experiment's (FOCUS-E831) data constitute the world's largest sample of many, if not most, charm decay processes. As a participant in FOCUS since its inception, UPR has designed and built detectors, monitored the data acquisition, played an important role in the primary data analysis and reduction and carried out several detailed physics analyses.

One of our principal projects for the future will be the construction of a new experiment (BTeV) that is designed to study chiefly CP violation in the B sector in a dedicated spectrometer at the Tevatron. BTeV has recently been recommended for construction by the HEPAP P5 subpanel. The plans for BTeV are detailed in a recent Technical Design Report (TDR). Preliminary work on BTeV was a major task during the project period.

The UPR physicists are members of the BTeV collaboration specifically in the subgroup charged with designing and building the muon detector. The group has specific responsibility for several tasks within the BTeV plans (Work Breakdown Schedule or WBS): (1) the construction of 1/3 of the muon detector modules, (2) the construction of the muon detector gas system, (3) the leadership of the muon detector software development.

Many physicists (not only in HEP) are learning that they need to become aware of the recent advances in statistics in order to improve their data analyses. On the other hand, the problems posed in high energy physics are also often open and challenging problems in statistics. Through a long-term collaboration between a statistician and a physicist, the UPR has been at the vanguard of the development of statistical techniques in HEP. The long-range plans are to play a significant role in the process whereby this research contributes to the improved analysis of major HEP experiments.

As a service to the HEP community, Dr. Lopez has taken on the responsibility of hosting the 2004 Heavy Quarks and Leptons Conference which will be held in San Juan, Puerto Rico.

1.1.1 Personnel

The Principal Investigator in this project was Dr. Angel Lopez. He is the Leader of the High Energy Physics Group at Mayaguez which is presently made up of two other faculty members and one Research Associate (Zhongchao Li). In addition, a faculty member from the Mathematics Department (Wolfgang Rolke) has been collaborating closely with Dr. Lopez for several years. Dr. Rolke is a statistician whose main line of research is directed towards improving the statistical techniques used in high energy physics.

During most of the project period Dr. Lopez served as a member of the High Energy Physics Advisory Panel (HEPAP) to which he was named by the Secretary of Energy. HEPAP is the highest ranking advisory body in the field of high energy physics. Another distinction for the PI was being chosen as Chairman of the 2004 Heavy Quarks and Leptons Conference.

Matching funds from the University of Puerto Rico permitted the hiring of a research associate for this project. That position was filled by an excellent young physicist, Dr. Zhongchao Li. Dr. Li received his PhD working on the BES experiment and he later worked on the L3 experiment at CERN for one year. He has experience in both hardware (BES trigger) and software analysis. There were typically three graduate students working with the project at any one time.

Graduate Student Training at UPR/Mayaguez

The project has had important consequences for the Physics Department of the UPR Mayaguez Campus which have translated into impacts on the quality of education at one of the main US minority institutions. This Department is the largest Physics Department in Puerto Rico with 100 undergraduate students and forty graduate students. The UPR itself is the leading Hispanic science and engineering (S&E) institution in the United States. Eighteen percent (18%) of the S&E PhDs granted to Hispanics nationwide are to students who have passed through the UPR either at the graduate or undergraduate level. The quality of the undergraduate students is high. Many could compete well in American universities but choose to stay in Puerto Rico due to cultural and economic reasons. The MS program receives high-quality students not only from Puerto Rico but from all of Latin America. Many of our BS graduates stay in Mayaguez to obtain a firmer base for their PhD studies in the U.S. at the same time that they improve their English skills. The same is true for the foreign students.

Name	Year	Current Position
Hugo Hernandez	**2002**	**PhD Candidate, U of New Mexico**
Eduardo Luiggi	**2003**	**PhD Candidate, Vanderbilt**
Alexis Paris	**2003**	**PhD Candidate, U of Pittsburgh**
Mauricio Penagos	**2003**	**Univ. Prof., Colombia**

Table 1.1: Students graduated from UPR High Energy Group

The highly advanced computer and electronics skills the MS students developed in this work will serve them well in the future. Of the four MS graduates from this project, three are currently in PhD programs at US institutions and one is teaching at a university in his home country (Table 1.1).

The opportunity for UPR students to involve themselves in world-class research at a national laboratory has had profound effects on the Department as well as the general research atmosphere on campus. This has been particularly important at this stage in the University's history when it is making the difficult transition from a purely teaching institution to an institution which also serves a research role. The students' presentations at Fermilab and the frequent interactions with our Fermilab collaborators are unique learning experiences which motivate them to higher achievement. Expectations are raised not only in the students directly involved but in their peers. There is a great deal of informal "technology transfer" to other Physics Department students and faculty that results from the HEP program. This is particularly true with respect to computing. We maintain a mini computing center dedicated to HEP which has the most sophisticated hardware and software in the College of Arts and Sciences.

1.1.2 Overview of SubProjects and Accomplishments

There are many topics that can be studied related to heavy quarks such as: production, spectroscopy, lifetimes, resonance structure in decays, semileptonic decays, mixing, CP violation and rare (or forbidden) decays. Fermilab's E687 charm photoproduction experiment which ran in 1988-91 carried out studies on all of these topics and has produced over 40 refereed publications. E687's follow-on experiment was FOCUS (an acronym for FOtoproduction of Charm with an Upgraded Spectrometer with some poetic license) which ran in 1996-97 with the ambitious goal of a tenfold increase in E687's statistics and a concurrent reduction in background. That goal was achieved. FOCUS (also known as E831) has reconstructed more than 1,000,000 charm events and has published 27 papers.

BTeV's main goal is the study of CP violation in the B sector where its effects should be large. CP violation is one of the most fundamental open questions in the Standard Model since it has only been studied in detail in the neutral kaon system. BTeV proposes a complete program for the study of CP violation which will be necessary in order to understand the effect fully. In addition, BTeV will carry out searches for forbidden and rare decays which can signal new physics and high-statistics studies of charm and B decays.

FOCUS Experiment

Based on its successful performance, the UPR has been playing an ever-expanded role in this experimental program. For FOCUS, the UPR responsibilities included four major systems: one of the muon detector stations, the muon trigger and two Cerenkov counters. All four systems were ready on time for the start of the run in July 1996. Our interest in muon physics led us to undertake the design and implementation of a first-level inner muon trigger and the refurbishing of the existing muon trigger counters. The recommissioning of two Cerenkov counters (C2 and C3) were major projects as was the development of a new algorithm for muon identification which minimizes misidentification of pions as muons. Contributions were made to the simulation of the inner muon system in FOCUS as well as to the development of routines related to the adjustment/calibration of the FOCUS muon and Cerenkov detectors. The group's contributions continued with monitoring of data acquisition and participation in the primary and secondary data reduction as well as with the development of simulation, data acquisition and analysis software. The UPR was solely responsible for the secondary skim of one of the main portions of the FOCUS data set, the leptonic stream.

The major accomplishments have been:

- Design, construction, installation and commissioning of a muon detector.
- Design, implementation and commissioning of a first level inner muon trigger.
- Refurbishing and recommissioning of two Cerenkov counters.
- Participation in the construction of the new hadron calorimeter.
- Significant participation in monitoring data acquisition.
- Development of an improved algorithm for muon identification.
- Development of simulation routines for the muon detector.
- Development of analysis tools for Cerenkov TDC information.
- Development of techniques to reduce the misidentification of other particles as muons using the data from the tracking system and the Cerenkov counters.
- Successful completion of a leptonic skim of 1,360Gb of data in Mayaguez.
- Search for the rare decay $D^0 \rightarrow \mu^+\mu^-$
- Measurement of the $D^+ \rightarrow \rho^0\mu^+\nu$ branching ratio.

BTeV

CP violation is one of the least tested aspects of the Standard Model. Although it has already been observed in the B sector, the most interesting tests will be made by second generation experiments with improved statistics which are only possible at hadron colliders.

BTeV expects to reconstruct more than 10^8 B decays per year. Much work has been done by the collaboration to design the most appropriate spectrometer for this purpose. This work is documented in the Technical Design Report. Physics simulations have been carried out using both MCFast (a Monte Carlo package developed by the Fermilab Computing Division for fast and flexible detector design studies) and GEANT. MCFast was used to determine the general characteristics of the baseline detector elements. GEANT simulation was used to do a more detailed design which was the basis for a detailed and realistic construction budget.

Dr. Lopez and his team carried out the bulk of the development of the GEANT simulation of the BTeV muon detector and has contributed significantly to the development of dimuon trigger algorithms. We have also collaborated in the construction of prototype muon detector units and in their beam tests at Fermilab.

Statistical Analysis

There have been major developments in the field of statistics in the last twenty years that have yet to be applied to problems in the analysis of high energy physics data. This subproject's overall goal was the development of analysis tools useful to a variety of HEP experiments but the approach was to do this by attacking specific problems which arose in the physics analysis of the actual data from the UPR experiments. Two NIM publications have resulted from this work and a third is on the way. They deal with the question of setting limits and finding signals in situations where there are low statistics. The direct collaboration between Drs. Lopez and Rolke ensured the excellent communication that was a prerequisite for the success of this interdisciplinary enterprise.

1.2 The BTeV Experiment

1.2.1 BTeV Physics Motivation

According to the Standard Model, CP violation is a consequence of the non-zero value of the phase parameter (η) in the Wolfenstein parameterization [1] of the CKM matrix. Assuming unitarity, this matrix depends only on four real quantities. The Standard Model postulates that this matrix applies to all quark weak decays. One can test this postulate with respect to CP violation by making several measurements which involve the CP violation parameter and checking for consistency. Several measurements are needed because typically a measurement will involve more than one parameter. Measurements in the K^0 system, test only a limited aspect of the Standard Model. A complete test requires measurements in the heavy-quark sector. For the B system, a different parameterization is usually used, that of the angles of the "unitarity triangle", the geometrical representation for the unitarity relationship which results from considering the orthogonality of the b and d columns of the CKM matrix. These angles α, β and γ are theoretically related to various measurements in the B system. Extraction of the values of these angles from the measurements is complicated by the fact that typically what is measured is $\sin(2x)$ where x is the angle. A single measurement thus suffers from a four-fold ambiguity on the value of x. Model dependence in the extraction of these angles in some measurements also leads to the conclusion that a systematic study of CP violation in many decay channels is necessary to answer the crucial question of the validity of the Standard Model for this phenomenon. BTeV intends to do such a study.

One of BTeV's main goals is to measure the angles α, β and γ precisely. First generation experiments such as Belle and Babar have already started the study of CP violation in the B system but there are many important measurements that BTeV will carry out for the first time. In particular, BTeV has a complete program for addressing the problem of the ambiguities in the measurements of these angles. In addition, BTeV will improve the precision of any existing measurements and carry out a precision study of B_s mixing. Another of BTeV's major goals is the search for rare final states from B decays, signals of new physics beyond the Standard Model.

According to the Standard Model, charm mixing and CP violating effects should be small. This is actually an excellent opportunity to discover new physics since any deviation from Standard Model predictions should be evident. BTeV will produce charm copiously enough to allow sensitivities

at or below Standard Model predictions for many channels even using a B trigger. The same can be said for rare charm decay searches.

Among the planned experiments or upgrades, only LHCb and BTeV have the capability of carrying out the full program of measurements which is necessary to do a detailed study of CP violation in the B sector. LHCb and BTeV complement each other well. BTeV has several advantages over LHCb which more than offset the difference in production cross section. The advantages come from the lower energy at the Tevatron together with the longer time between beam crossings (132 ns vs 25 ns at the LHC) and several BTeV design features. (See Section 1.2.2 .) The lower energy means that there is less combinatoric background and larger opening angles in B decay which translate into fewer acceptance losses in the beam direction (products going down the beam pipe). The lower track multiplicities also reduce radiation damage; the vertexing detector can be placed closer to the beam. The lower energy also means that BTeV can be a smaller and less expensive detector. The longer time between crossings has several advantages the main one being that it permits a Level-1 detached vertex trigger which has no final-state biases. Besides the vertexing trigger, BTeV's unique features include a magnetic field in the central region and a high resolution electromagnetic calorimeter.

Heavy Hadron Lifetimes

Lifetime of Charmed Hadrons In a zero order approximation, the lifetime of a particle containing a heavy flavor quark can be estimated with the "Spectator Model". In this process, it is assumed that while the heavy quark decays to a lighter quark, and radiating a virtual W-boson, the remaining constituents of a hadron (like u, d or s) are spectators and do not participate in the process. The decay rate of the heavy quark increases very quickly with its mass ($\Gamma \propto m_Q^5$). In this model, the heavy particle decays by radiating a W, as shown in Figure 1.1. From this model a rough estimate of the quark charm lifetime

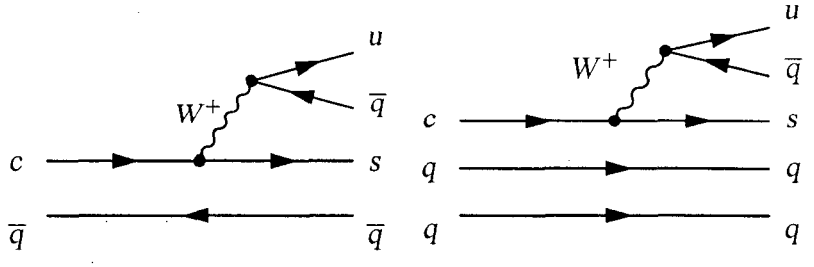

(a) Heavy Meson decay. (b) Heavy Baryons decay.

Figure 1.1: Feynman diagram for the External Decay of a Charmed Hadron, to visualize the Spectator process.

(scaling from muon decay) is given by

$$\tau_C \simeq \tau_\mu \frac{1}{5}(\frac{m_\mu}{m_C})^5 \sim 0.8 \text{ ps}, \tag{1.1}$$

where m_μ is the mass of the muon, and m_c is the mass of the charm quark. The factor of $1/5$ accounts for the two leptons (electron and muon) and three quark colors into which charm quark can decay. This result is consistent with the average of the experimental lifetime of D^+ and D^0 which is about 0.73 ps. Although the Spectator Model gives a reasonable estimate for the order of magnitude of charmed hadron lifetimes, it is unable to predict the large lifetime differences seen experimentally between different weakly decaying bound states. The longest (D^+) and the shortest (Ω_c^0) lifetimes differ by a factor of about 15. In order to model these differences, additional effects must be considered.

Charmed Mesons From recent FOCUS experimental results the ratio of the D^+ lifetime to the D^0 lifetime is 2.538 ± 0.023 [2]. If one combines this result with the branching ratio of semi-leptonic decays [3] we find the D^+ and D^0 semi-leptonic decays widths are nearly equal.

$$\frac{\Gamma(D^0 \to e^+X)}{\Gamma(D^+ \to e^+X)} = \frac{\mathrm{BR}(D^0 \to e^+X)}{\mathrm{BR}(D^+ \to e^+X)} \times \frac{\tau(D^+)}{\tau(D^0)} = 1.00 \pm 0.12 \tag{1.2}$$

This last result implies that any differences in lifetimes are due to hadronic decays.

At the end of 1979 several non-leptonic processes were studied which could contribute to the differences in lifetimes. To explain the unexpected D^+/D^0 lifetime difference two sources were found to be important [4], "Weak annihilation" (WA)[1] and "Pauli Interference" (PI). WA is not a "spectator" process; it is a term in addition to the Spectator Model. PI is a correction to, or a fine tuning of, the Spectator Model.

The WA rate (See Figure 1.2) is present in Cabibbo favored (CF) decays of the D^0 mesons, but does not contribute to CF D^+ decays. However the WA rate is doubly suppressed relative to spectator rate. It is helicity suppressed by a factor $(m_s/m_c)^2$ and 'wave function overlap' suppressed by a factor $(f_D/m_c)^2$. This suppresion is so large that WA alone cannot account for the D^+/D^0 lifetime difference. Therefore a second effect which was initially disregarded became apparent.

The second effect is the Pauli Interference that occurs when there are two identical quarks in the final state. The PI effect is present in Cabibbo favored D^+ decays but not in D^0. PI causes the D^+ to decay more slowly, because of destructive interference coming from the exchange of two identical antiquarks, the $\bar{d}$ valence antiquark with the $\bar{d}$ from the c decay ($c \to s\bar{d}u$). This interference can be visualized as the interference between the external and internal spectator diagrams shown in Figure 1.3. Both diagrams give the same final state, but the internal spectator decay is color suppressed.

Charmed Baryons Similarly, for charmed baryons, the simple spectator model was expanded by three additional terms: "W Scattering" (WS) which is similar to WA, and PI (constructive and destructive). In baryons, unlike mesons, these mechanisms are neither color nor helicity suppressed. The Pauli interference term is computed to be constructive when the quark from charm quark decay matches a spectator quark (The exchange of s quarks in Figure 1.4(b)). The interference is computed to be destructive when a quark coming from the decay of the virtual W matches a spectator quark (The exchange of u in Figure 1.4(b)). These contributions are shown in Figure 1.4.

[1] The distinction between W exchange in the t channel with weak annihilation in the s channel is artifi cial, because the two operations are mixed under QCD renormalization, although D_s^+/D^0 lifetime differences may reveal some difference between these two diagrams. Both cases will be referred to as WA.

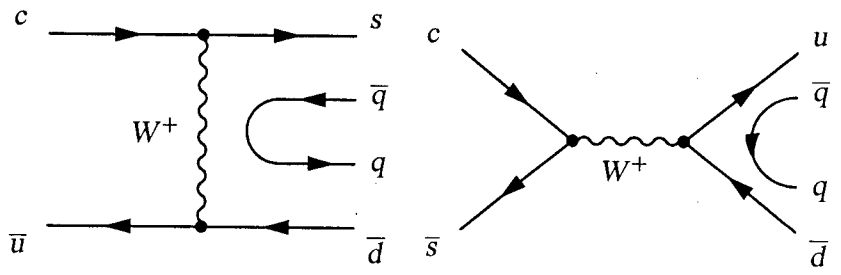

(a) W Exchange. (b) Annihilation.

Figure 1.2: These diagrams comprise the non-spectator Weak Annihilation contributions to the charm mesons lifetime. Both are helicity and wave function suppressed. Both are non-leptonic decays.

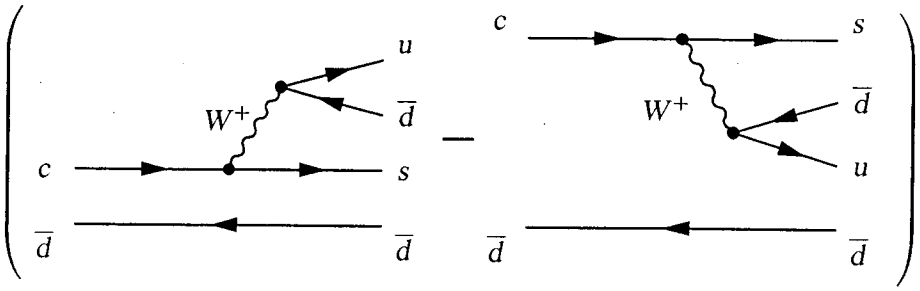

Figure 1.3: The interference of these two diagrams (external and internal spectator) represents the PI in the D^+ decay. The minus sign represents the destructive interference between the diagrams.

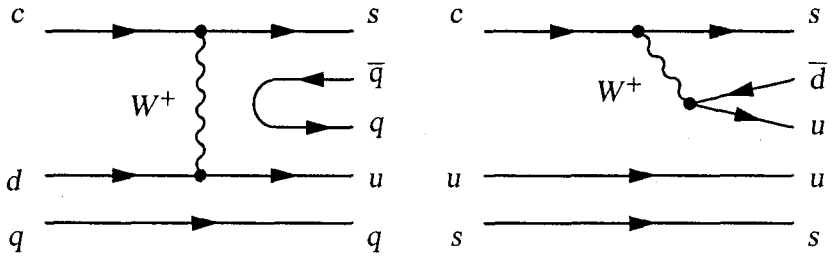

(a) W Scattering. (b) Internal Spectator.

Figure 1.4: Feynman diagrams which contribute to charm lifetimes. These diagrams comprise the non-spectator contributions to the charm baryon lifetime, and depend on the initial quark content.

In baryons, the dominant amplitudes to Cabibbo favored hadronic decays are the external spectator (Figure 1.1(b)), the internal spectator (Figure 1.4(b)) and the W scattering (Figure 1.4(a)). The rate of the spectator process is given by the sum of the rates of the external and internal spectators. The interference terms of the amplitudes are better approximated as two terms, the interference due to the u quark which is computed to be destructive and the interference of the s which is computed to be constructive. (In mesons the interference term is due to the $\overline{d}$ quark and it is computed to be destructive). In general, interference terms are constructive or destructive depending on the spin-color arrangement of the produced quarks relative to the spectator quarks, and can be found only by computing the specific dynamics.

The contributions to the Cabibbo favored hadronic decays for various charmed hadrons are given below:

$$\begin{aligned}
\Gamma_{NL}(D^+) &= \Gamma_{\text{spc}} - \Gamma_{\text{int}}^- \\
\Gamma_{NL}(D^0) &= \Gamma_{\text{spc}} + \Gamma_{\text{WA}} \\
\Gamma_{NL}(D_s^+) &= \Gamma_{\text{spc}} + \Gamma_{\text{WA}} \\
\Gamma_{NL}(\Lambda_c^+) &= \Gamma_{\text{spc}} - \Gamma_{\text{int}}^- + \Gamma_{\text{WS}} \\
\Gamma_{NL}(\Xi_c^+) &= \Gamma_{\text{spc}} - \Gamma_{\text{int}}^- + \Gamma_{\text{int}}^+ \\
\Gamma_{NL}(\Xi_c^0) &= \Gamma_{\text{spc}} + \Gamma_{\text{int}}^+ + \Gamma_{\text{WS}} \\
\Gamma_{NL}(\Omega_c^0) &= \Gamma_{\text{spc}} + \tfrac{10}{3}\Gamma_{\text{int}}^+
\end{aligned} \tag{1.3}$$

where Γ_{spc} is the contribution due to the spectator decay process, Γ_{WS} (Γ_{WA}) is the contribution of W Scattering (Weak annihilation in mesons) and $\Gamma_{\text{int}}^+(\Gamma_{\text{int}}^-)$ is the contribution due to constructive (destructive) interference. The interference term for the Ω_c^0 is enhanced due to the presence of three final state s quarks which interfere with each other [5], compared to the Ξ_c^+ or Ξ_c^0. The numerical factor $\frac{10}{3}$ is due to the spin wave function.

In the nineties, a long and difficult theoretical development resulted in the robust *Heavy Quark Expansion* (HQE) theory (See Reference 6 and references therein). In this theory non-

perturbative corrections are put together in a systematic expansion in inverse powers of the heavy quark mass $(1/m_c)^n$, through a technique named *Operator Product Expansion* (OPE). The weak decay is expressed as:

$$\Gamma(H_c \to f) = \frac{G_F^2 m_c^5}{192\pi^3} |V|^2 \frac{1}{2M_{H_c}} \times \left[\sum_{D=3}^{\infty} c_D^f \frac{\langle H_c|O_D|H_c\rangle}{m_c^{D-3}}\right] \tag{1.4}$$

Where H_c is the heavy hadron, f is some final state, G_F is the Fermi coupling constant, V is the CKM matrix element present in the decay, M_{H_c} is the mass of hadron containing the heavy quark, D is the dimension of the operator O_D, c_D^f are the coefficients of the series.

The theory is based on:

i) a systematic expansion of amplitudes in the inverse mass of the heavy quark (m_c^{-1}).

ii) estimates of matrix elements of local operators (appearing in the expansion) over the hadronic states H_c.

The first condition (i) takes into account the quark-gluon dynamics at short distances and is based on fundamental QCD. The second condition (ii) about the hadronic matrix elements reflects the hadron structure at long distance, and is "limited" because some relevant matrices are not calculable theoretically; the values must be extrapolated or interpolated from related experimental results. This is why measurements of b-baryon lifetimes are crucial for development of the theory.

HQE successfully predicts qualitatively the lifetime hierarchy in the charm particles:

$$\tau(D^+) > \tau(D_s^+) \sim \tau(D^0) \geq \tau(\Xi_c^+) > \tau(\Lambda_c^+) > \tau(\Xi_c^0) \sim \tau(\Omega_c^0) \tag{1.5}$$

A number of authors [7–10] predict that $\tau(\Xi_c^+)/\tau(\Lambda_c^+) \sim 1.3 - 1.6$. But experimentally using FOCUS data a ratio of $\tau(\Xi_c^+)/\tau(\Lambda_c^+) = 2.15 \pm 0.13$ is obtained [11–13], and is supported with the CLEO result of $\tau(\Xi_c^+)/\tau(\Lambda_c^+) = 2.8 \pm 0.3$ [14].

Lifetimes of Beauty Hadrons The calculations of HQE can be applied to the b quark sector. HQE is expected to work better at higher masses, and for instance better predictions compared with charm are expected for the b sector. Much has been learned about B-mesons, largely from CLEO, CDF, Babar, Belle and LEP [3]. However, discrepancies between theory and experiment are still present, both for B-mesons and B-baryons [15].

The contributions to the Cabbibo favored hadronic decays for various b hadrons are given below, similarly to the charm case.

$$\begin{aligned}
\Gamma_{NL}(B^+) &= \Gamma_{\text{spc}} - \Gamma^-_{\text{int}(u)} \\
\Gamma_{NL}(B^0) &= \Gamma_{\text{spc}} + \Gamma_{\text{WA}(d)} \\
\Gamma_{NL}(B_s^0) &= \Gamma_{\text{spc}} + \Gamma_{\text{WA}(s)} \\
\Gamma_{NL}(B_c^+) &= \Gamma_{\text{spc}} + \Gamma_{\text{int}(c)} \\
\Gamma_{NL}(\Lambda_b^0) &= \Gamma_{\text{spc}} + \Gamma_{\text{WS}(u)} - \Gamma^-_{\text{int}(d)} \\
\Gamma_{NL}(\Xi_b^0) &= \Gamma_{\text{spc}} + \Gamma_{\text{WS}(u)} - \Gamma^-_{\text{int}(s)} \\
\Gamma_{NL}(\Xi_b^-) &= \Gamma_{\text{spc}} - \Gamma^-_{\text{int}(s)} - \Gamma^-_{\text{int}(d)} \\
\Gamma_{NL}(\Omega_b^-) &= \Gamma_{\text{spc}} - \tfrac{10}{3}\Gamma^+_{\text{int}(s)}
\end{aligned} \tag{1.6}$$

For B baryons there are only Λ_b^0 experimental results. The best measurement is based on about 150 events in semileptonic decay $\Lambda_c l\nu$ by DELPHI. [16]. The sample is b-baryon dominated by Λ_b production.

While the lifetime agrees qualitatively with theory expectations, one data point cannot provide the pattern of lifetimes necessary to understand B-hadron decays. So far, at least for mesons, all is well within experimental uncertainty. The theory predicts for b hadrons the following pattern for the lifetime hierarchy in the beauty hadrons [17]:

$$\tau(B_c) << \tau(\Xi_b^0) \sim \tau(\Lambda_b^0) < \tau(B_d^0) \sim \tau(B_s^0) < \tau(B^-) < \tau(\Xi_b^-) < \tau(\Omega_b) \qquad (1.7)$$

From this pattern very few points have been tested experimentally. And there is already a discrepancy in the ratio $\tau(B)/\tau(\Lambda_b^0)$ between theory and experiment. More measurement points will help to understand the source of this discrepancy, for which there is no explanation at this time.

1.2.2 BTeV Background

The BTeV Spectrometer

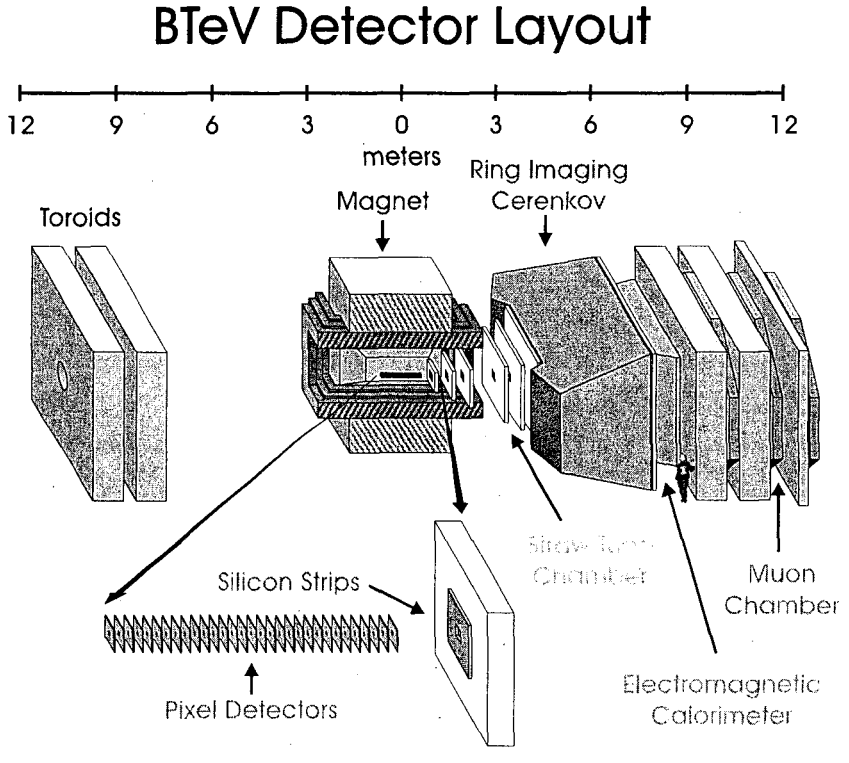

Figure 1.5: BTeV/C0 Spectrometer

The key features of the baseline design (Fig. 1.5) are: (1) a dipole analyzing magnet surrounding the IR, (2) a precision planar pixel vertex detector, (3) a Level 1 vertex trigger, and (4) excellent particle identification provided by a RICH counter, a muon proportional tube system and

a high quality $PBWO_4$ electromagnetic calorimeter. BTeV is designed to look at $B\bar{B}$ pairs going in the forward direction, where the B and $\bar{B}$ are strongly correlated to have a small opening angle. (By forward we mean either the p or $\bar{p}$ beam direction.) All of the physics, including B tagging, can be done with just one arm . In fact, fiscal considerations required that the detector be downsized from its initial two-arm to a one arm design. However, this did not affect any of BTeV's intrinsic capabilities. The pixel detector consists of a total of 4.2×10^7 channels arranged in 100 transverse planes (10cm square) spaced along a longitudinal distance of 1m. (The IR is currently planned to have a σ of 30cm.) The beam hole through the center of each plane is only 12mm square so the detector must withstand high radiation levels. Each pixel is $50\mu m \times 400\mu m$ aligned either along the bend or non-bend direction. The vertex trigger is designed for high efficiency for most heavy-quark events even those without leptons. It should reduce the event rate by a factor of 100 starting from an interaction rate of 15MHz at a luminosity of $2 \times 10^{32} cm^{-2} s^{-1}$. This is achieved by using a heavily pipelined and parallel processing architecture which allows a decision time of $33\mu s$ (could be made longer if necessary). Charged hadron identification in the range from 3-$70GeV$ is provided by a C_4F_{10} RICH which is 3m long. The electromagnetic calorimeter is capable of detecting final states with single photons, π^0s, ηs or η's.

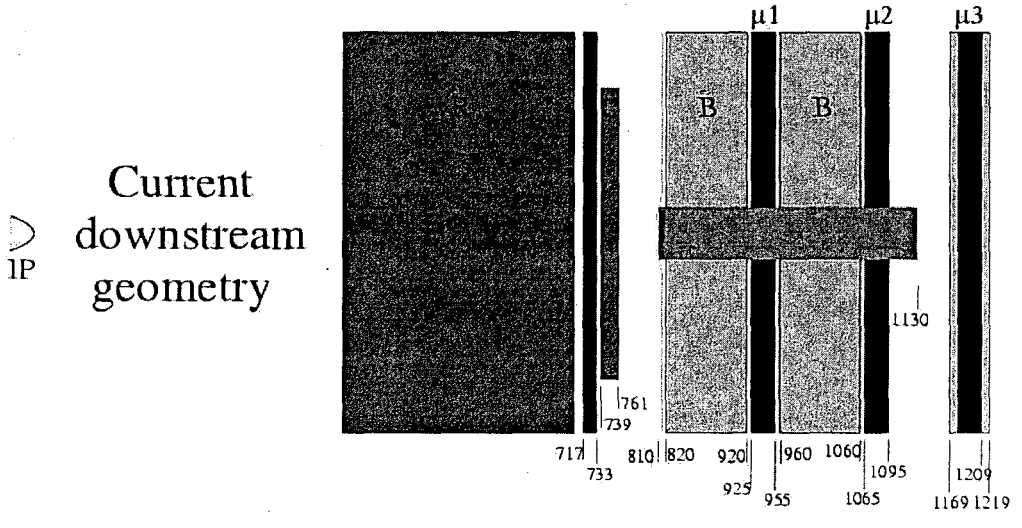

Figure 1.6: BTeV Muon System Geometry

The Muon Detector The muon detector is designed to do stand-alone momentum/mass triggering, to withstand rates of a few kHz/cm^2 in the parts closest to the beam, to have fairly uniform occupancy and to have a time resolution of less than 60 ns in order to reject backgrounds related to the beam passing through the hole in the detector before reaching the interaction region. The baseline design consists of two 1m toroidal (1.5T) filters with three proportional tube measuring stations (Fig 1.6). The two stations after the second filter provide most of the information necessary for the momentum measurement. The station between the filters mainly serves to reject backgrounds by confirming the others.

Figure 1.7: (left) Beams-eye view of one muon detector station, which consists of eight overlapping octants arranged in two layers. One octant is cut away in places to show the overlap between adjacent octants. (right) Arrangement of planks to form the four views in an octant (r view is repeated). There will be 12 planks per octant (more than shown).

Each station is composed of eight overlapping pie-shaped "octants" (Fig 1.7) which contain four views each composed of a double layer of proportional tubes with an offset of half a tube in a "picket-fence" arrangement. In all four views the planks are shorter near the beam pipe (where particle fluxes are highest) and get longer at larger radii. The tubes vary from 1 to 6 feet in length. Two of the views are radial (r) views which provide the most important bend information. The second r view provides redundancy and helps to reject fake tracks. The other two views (u) and (v) are each rotated 22.5^0 with respect to the r views.

The tubes are 3/8" diameter thin-walled stainless steel bundled in "planks" of 32 (Fig 1.8) with a common gas manifold and electrical connectors. There are thirteen planks in each view of an octant. Mechanically two octants are mounted together to form a "quadrant" which is the unit that is moved in and out of the spectrometer. The total channel count is 36,864 for one arm.

The 0.5 cm effective wire pitch per plank results in a position resolution of 1.4 mm in the toroidal bend view and 2.8 mm in the azimuthal direction (using the information from all views). Signal amplification and digitization are done by integrated circuits mounted on boards connected directly to each plank. In order to meet the timing requirements only the first 6-8 ns of the charge coming from the ion drift are integrated. Further signal processing (data compression and conversion to optical format) are done on boards located in the experimental hall in order to reduce long cable runs.

Project Contributions to BTeV

Dr. Lopez is one of the original members of the BTeV collaboration and, as such, has been working in the muon detector development effort since its beginning. Our group carried out the bulk of the development of the GEANT simulation of the BTeV muon detector. In addition, we generated roughly half of the GEANT simulation data which was used in the detailed study of the dimuon trigger algorithms including an independent dimuon trigger algorithm developed at UPR. Details of the results of this work can be found in the Appendix A.

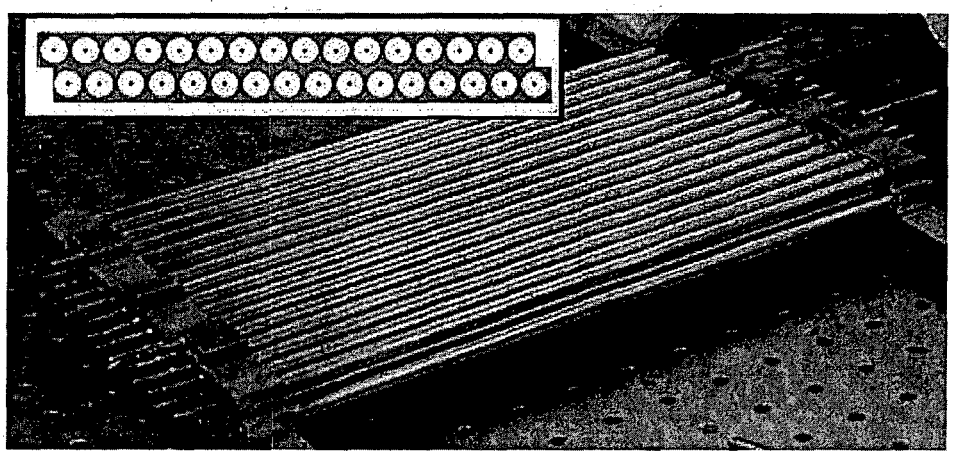

Figure 1.8: The basic building block of the muon system (plank). The inset shows an end view of the plank, and demonstrates the "picket fence" geometry of the proportional tubes. The gold colored pieces at each end of the plank are the brass gas manifolds. Visible at the end is the circuit board soldered around the edge to the brass piece.

The current plan for the BTeV muon trigger algorithm was developed at the Univ. of Illinois but it follows the spirit of the original UPR algorithm by using simple correlations between the muon hits in different stations. Recently we have developed an analytical model which allows us to calculate the parameters that appear in these correlations. This work can be found in Appendix B.

Concurrent with the development of simulation tools, an active BTeV detector R&D project has complemented the simulation. The main emphasis has been on the pixel detector but all detector groups have been busy building prototypes. In particular, there has been considerable work on the muon detector whose detailed design is documented in the BTeV TDR. At UPR we have collaborated in this design effort and were heavily involved in the construction of prototype muon detector units and in their beam tests at Fermilab during the summer of 2001. The results of this work can also be found in Appendix A.

Another major task was the design of the muon detector gas system. UPR/RUM will build the gas mixing, monitoring and delivery system for the muon detector. The current plan is to use an Argon–CO_2 mixture, probably in the ratio 85:15. Gas studies at Vanderbilt have determined that this mixture provides a wide plateau region which makes it forgiving of variations in pressure, temperature, etc. This gas is also fast enough to ensure that ionization from adjacent beam crossings (a minimum 132 ns apart) will not be picked up with high efficiency. Finally, Ar–CO_2 is inorganic and does not suffer from hydrocarbon build up which is seen in high rate detectors which use organic gases, e.g. Argon–Ethane. Evidence for wire chamber aging in high-rate environments even with Ar–CO_2 has been found which is postulated to come from contaminants. We plan to minimize the contaminant problem in several ways. First, the entire gas system will be made of metal (copper, brass, and/or stainless steel) which is much more inert than plastic products. Second, we plan to test the delivered Argon and CO_2 gas. Third, we will monitor the gas gain continuously using a gas gain monitor with an Fe-55 source as shown in Fig. 1.9. Finally, we will use a gas mass spectrograph to check the mixing and to check for impurities in the gas.

The gas system starts with pure Argon and CO_2 which are mixed in a mixing system. The

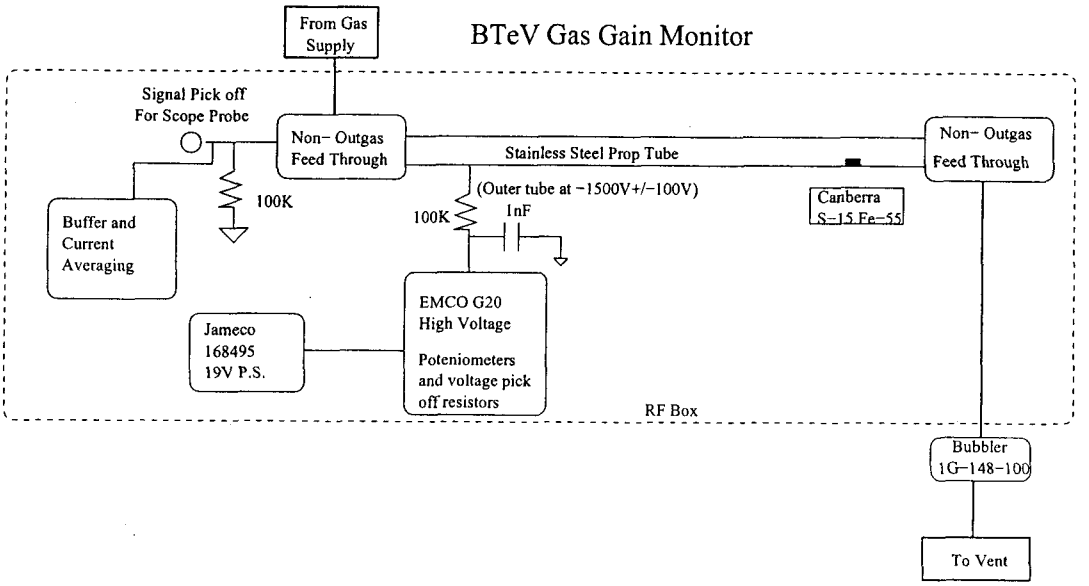

Figure 1.9: Design of gas gain monitor for the muon detector in the BTeV experiment.

gas flow is split several times in several different manifolds until reaching the planks. Gas flow will be completely parallel, that is, no gas will go through more than one plank. The gas system will be designed to allow up to 5 gas volume exchanges per day. We show the design for the gas mixing system in Fig. 1.10 and the design for the overall gas system in Fig. 1.11.

We will also utilize gas gain monitors to monitor the gas gain over time. These will be placed at the input and output ends of the gas system and will be composed of single tubes and an Fe-55 source.

1.3 The FOCUS Experiment

Background on the FOCUS experiment and on UPR's early contributions to FOCUS can be found in Appendix C.

1.3.1 FOCUS Physics Motivation

There has been a considerable amount of progress in charm physics during the last two decades both on the experimental as well as the theoretical side. Two experimental groups have been particularly successful in continually increasing the statistical power of charm samples by upgrading their spectrometers. These are the E687-FOCUS family of experiments and the CLEO clan with its many generations. On the theory side, the development of heavy quark effective theory as well as continued improvements in lattice gauge calculations have provided ways to improve the precision of

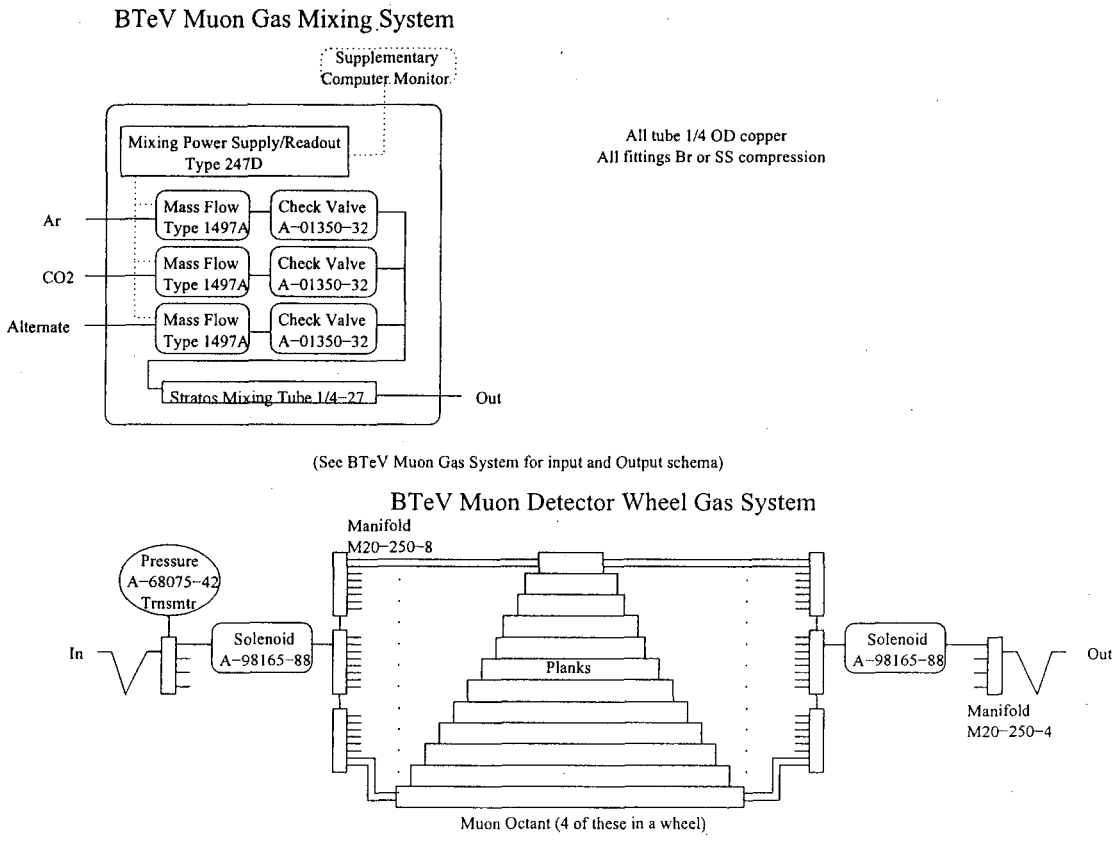

Figure 1.10: The design of the gas mixing system (left), and the delivery schema to the collection of detector planks on an octant.

theoretical predictions in spite of the non-perturbative nature of the color interaction that binds quarks into hadrons with important effects on the production and decays of charmed hadrons.

The net result is that the charm sector provides an excellent testing ground for our existing theory. The observation of mixing in charm would be of great importance because it would be a hint of new physics beyond the standard model. Measurement of charm lifetimes are critical input parameters for several theory models, allowing better quantification of non-perturbative QCD. Semileptonic decays can be used to test lattice gauge calculations and quark models and for the measurement of CKM matrix element ratios such as $|V_{cd}/V_{cs}|^2$.

Although there are many physics topics that can be studied using charm, we will only discuss here the search for new physics by looking for rare and forbidden decays since this is one of our main topics of interest. In the Standard Model there are no known gauge interactions corresponding to the assumptions of conservation of lepton number and of lepton flavor. In fact, the recently discovered neutrino oscillations strongly suggest that lepton flavor conservation is not an exact symmetry. It is of interest to find other instances of such Standard Model "forbidden" processes.

Flavor changing neutral currents (FCNC), on the other hand, are examples of rare decays. In the Standard Model, these are suppressed by the GIM mechanism whereby the tree level diagrams

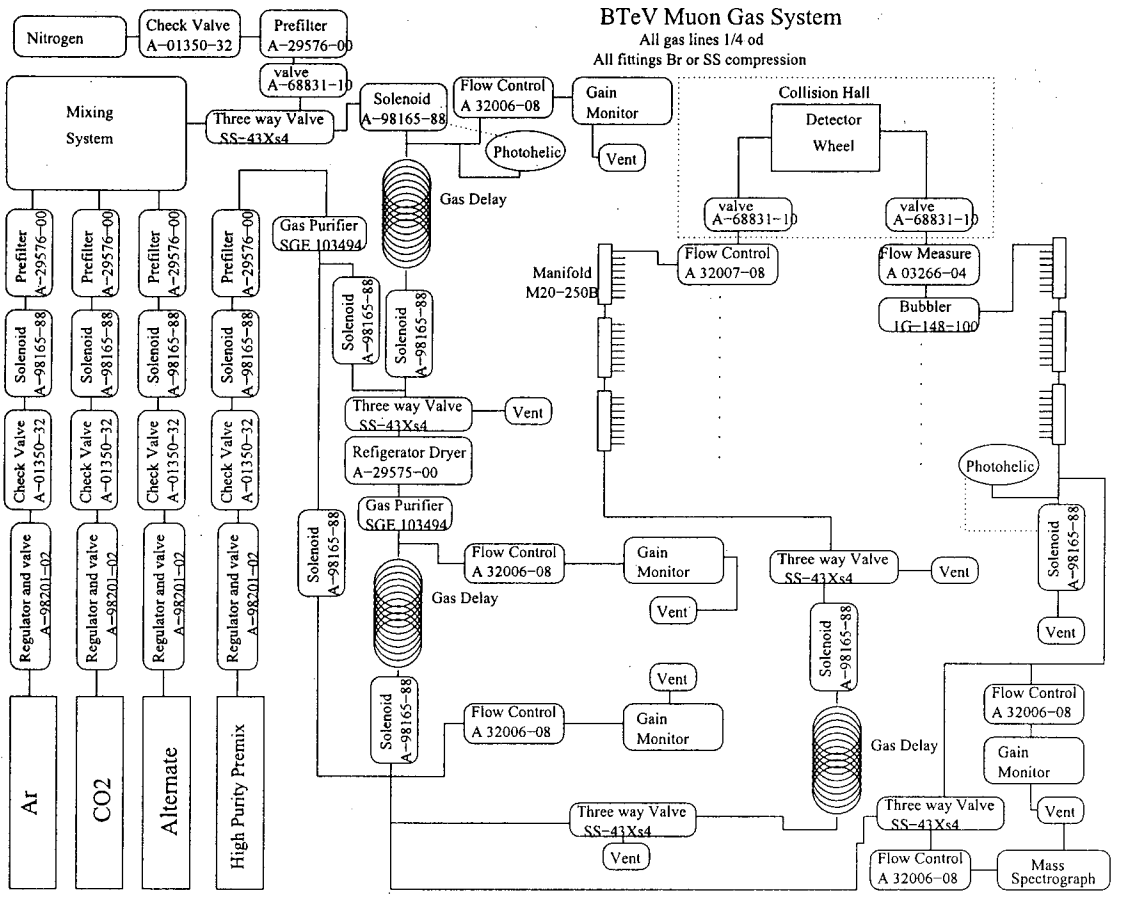

Figure 1.11: The overall design of the gas system. There are redundant layers of monitoring and delivery.

cancel and the predicted rates are exceedingly small. This is actually an excellent opportunity to observe the effects of new physics since they will not be masked by Standard Model processes. Table 1.2 gives examples of rare or forbidden charm decays including lepton number violating decays (LNV) and lepton flavor violating decays (LFV).

1.3.2 UPR Recent Contributions to FOCUS

Semileptonic Decays

The analysis of the $D^+ \to \rho^0 \mu^+ \nu$ decay was essentially completed this year. The details can be found in Appendix D. This analysis is very difficult due to the necessity of developing effective selection criteria to control the large number of copious backgrounds. In addition to the usual difficulties inherent to a semileptonic analysis, the extremely difficult background environment is due to the large width of the

Decay	Type
$D^0 \to l^+l^-$	FCNC
$D^+_{d,s} \to h^+l^+l^-$	FCNC
$D^0 \to \mu^\pm e^\mp$	LFV
$D^+_{d,s} \to h^+\mu^\pm e^\mp$	LFV
$D^+_{d,s} \to h^-\mu^+e^+$	LFV
$D^+_{d,s} \to h^-l^+l^+$	LNV

Table 1.2: Rare and Forbidden Decays. l is lepton; h is π or K. FCNC= flavor changing neutral current(rare); LFV = Lepton-Flavor violating(forbidden); LNV= lepton-number violating(forbidden)

ρ^0 and to the numerous sources of pions which can mimic the dipionic ρ^0 decay. The full power of the FOCUS detector was brought to bear specially in the particle identification using the Cerenkov and muon systems. The analysis used the real data as much as possible to obtain information on backgrounds specially their mass distributions. In fact, a reskim of 10% of the complete FOCUS data was done in order to study backgrounds from muon misidentification.

The signal yield is obtained from a three-parameter fit to the dipion invariant mass distribution. The fitting function includes nine different background sources. Even with such a complicated fit, the methodology is shown to be very stable in a detailed systematic study that is also found in Appendix D.

A Search for the Rare Decay $D^0 \to \mu^+\mu^-$

Appendix E presents the details of this analysis which is essentially complete. Besides using the full capability of FOCUS for muon identification, the analysis incorporated statistical techniques developed at UPR including the implementation of the dual bootstrap methodology [19] and the calculation of the effect of systematic uncertainties.

1.4 Statistical Analysis

In this subproject Dr. Lopez and Dr. Rolke have been collaborating in the improvement of some of the methods currently used in the statistical analysis of high energy physics data. This collaboration has resulted in six publications, including an official FOCUS publication where several of their methods were used in the analysis of rare and forbidden 3-body dimuon decays of the charmed mesons D^+ and D^+_s. Two more publications are in preparation.

1.4.1 A Frequentist Approach to Nuisance Parameters

In recent years many researchers in high energy physics have encountered the problem of quoting limits in situations with very few, or even no, observations. For example, this is often the case in the search for new physics or even expected physics which is being seen for the first time (such as the initial top observations). This problem has therefore attracted a great deal of attention in the high energy physics community, and a number of methods such as [20] have begun to appear. We have developed a method for including the background uncertainty in the computation of the limits. This work was published in Rolke and López (A) [21]. This is an example of a more general problem when finding limits, namely how to deal with nuisance parameters such as the background rate or the efficiency. This problem was one of the major issues discussed at the recent PHYSTAT2003 conference at SLAC.

Let us consider the problem of finding limits for the signal rate in the presence of background, with the exact background rate unknown. If we use sidebands to estimate the background rate we find the following probability model:

$$X \sim Pois(\mu + b), \qquad Y \sim Pois(\tau b)$$

where X is the number of events found in the signal region, Y is the number of events in the data sidebands, μ is the signal rate, b is the background rate and $Pois$ is the usual Poisson distribution. τ is the probability for a background event to fall into the background region divided by the probability that it falls into the signal region, and therefore Y/τ is the estimated background rate. The loglikelihood for this model is then given by

$$l(\mu, b; x, y) = x \log(\mu + b) - (\mu + b) - \log(x!) +$$

$$y \log(b) - \tau b - \log(y!)$$

The idea of the profile likelihood is to find for each μ the b that maximizes the loglikelihood. In the case here this can means solving the equation

$$\frac{\partial}{\partial b} \log l(\mu_0, b; x, y) = \frac{x}{\mu_0 + b} - 1 + \frac{y}{b} - \tau \doteq 0$$

which has the solution

$$\widehat{b} = \frac{x + y - (1+\tau)\mu_0 + \sqrt{(x + y - (1+\tau)\mu_0)^2 + 4(1+\tau)y\mu_0}}{2(1+\tau)}$$

A theoretical argument for the profile likelihood is as follows: confidence intervals can often be found by inverting a corresponding hypothesis test. Here this is a test of

$$H_0 : \mu = \mu_0 \text{ vs. } H_a : \mu \neq \mu_0$$

The likelihood ratio test statistic for this hypothesis test is given by

$$\Lambda(\mu_0; x, y) = \frac{\max\{l(\mu_0, b; x, y) : b \geq 0\}}{\max\{l(\mu, b; x, y) : \mu \geq 0, b \geq 0\}}$$

and the numerator of this expression is simply the loglikelihood evaluated at the profile likelihood.

1.4.2 Bias-Corrected Confidence Intervals

In recent years researchers in high energy physics have come to realize that some of the standard analysis techniques carry with them the danger of introducing a bias. One major example is the search for a cut combination which eliminates background events but retains as many signal events as possible. This can lead to using a cut combination which is optimal for the data set at hand, but not for the process that generated the data set, and that therefore depends too much on random fluctuations in the data. A good way to lower the risk of introducing this bias is by performing a blind analysis, whereby the choice of cut is solely based on the background sidebands or on simulated background. It should be clear, though, that this only alleviates half the problem: we no longer are subject to upfluctuations in the signal region, but we are still in danger of optimizing our cut on a downfluctuation in the sideband or simulated background.

The source of the remaining problem can be understood to be the fact that we are using the same data to do two things: to choose the cut set and to estimate the background level. One attempt at dealing with this is to use split samples: randomly divide the data into two parts, use one part to find the optimal cut combination, use the other to find the limits. This approach has two major flaws: first there is the question of what the relative size of the two parts should be, and then there is the problem that the parts have even lower statistics than the whole, thus worsening the effects of fluctuations.

We have used a variant of the statistical bootstrap to minimize this bias. The choice of a cut combination is usually based on an optimality criterion. One possible optimality criterion is the experimental sensitivity, a variable which is derived from the sensitivity defined in Feldman and Cousins [20] and in Review of Particle Physics [22]. The experimental sensitivity is defined as the average of the upper limits that would be quoted for an ensemble of experiments with no true signal. It can be thought of as a measure for the size of an effect that could be discovered by a certain experiment. The smaller the experimental sensitivity of a cut set, the more likely we are to discover a signal that is truly present.

In ASAT [23] and Rolke and Lopez B [19] we showed that even doing a blind analysis there is still a bias, leading to confidence intervals that severely undercover. This was done by performing a Monte Carlo study based on real FOCUS data, specifically the $D^0 \to \mu^+\mu^-$ decay. We generated fake data sets using the FOCUS Monte Carlo, with varying signal and background rates. Then we applied each of 13122 cuts to the data and found the cut with the smallest experimental sensitivity. Using that cut we found the confidence interval (or upper limit) for the signal rate using Rolke and Lopez A [21].

The method of Rolke and Lopez A [21] is the only method currently known that treats the uncertainty in the background rate as a statistical error. Feldman and Cousins [24] independently solved this problem, and proposed a modification to their solution. Like Feldman and Cousins [20] the Rolke-Lopez method solves the "flip-flop" problem, and it always results in physically meaningful limits. The problem described here as well as its solution, though, do not depend on what method of computation is used for either the sensitivity or the limits. As long as there is some uncertainty in the background rate, the bias would be equally present if we had used, for example, Feldman and Cousins [20] or a Bayesian method.

In order to adjust for this bias we then proposed a variant of the statistical bootstrap: here one draws one bootstrap sample from the data and finds the cut with the smallest sensitivity for this bootstrap sample, then one draws another bootstrap sample, independent from the first, to find the limits. This procedure is then be repeated B times, with a B of about 5000. In this manner one gets B

lower and upper limits. Finally the median of the lower and the median of the upper limits is used as the estimates.

In this way for each bootstrap sample one gets a cut set that is optimal for the first bootstrap sample but not necessarily for the second, which is representative of the underlying distribution, and one can therefore expect to get unbiased estimates for the limits or, in other words, limits with the correct coverage rate.

Repeating the MC study discussed above but now using this dual bootstrap method, one gets the dotted in line in Figure1. This shows that the dual bootstrap method yields limits with the correct coverage, effectively removing the minimization-evaluation bias.

The statistical bootstrap method in general is a non-parametric alternative for finding error and bias estimates in situations where the assumption of a Gaussian distribution is not satisfied and where it is difficult or even impossible to develop an analytic solution. It was first developed by B. Efron in [25]. Since then a great deal of theoretical work has been done to show why and when the bootstrap method works, see for example Hall [26], and it has been successfully used in a wide variety of areas. Previous applications of the bootstrap in High Energy Physics can be found in Hayes, Perl and Efron [27] and in Alfieri et al. [28]. For a very readable introduction to the subject see Efron and Tibshirani [29].

Correct coverage is not the only characteristic a good method should have. It is also important to obtain the strictest limits possible. That is what the minimum sensitivity cut methodology attempts to do, and using a blind analysis together with the dual bootstrap we showed that this yields confidence intervals with the correct coverage.

1.5 Heavy Quarks and Leptons 2004

The workshop "Heavy Quarks at Fixed Target" belongs to a series of conferences initiated at INFN Laboratori Nazionali di Frascati in 1993. The subsequent editions have been held at University of Virginia, Charlottesville (1994); at St. Goar, Germany (1996); at Fermilab, Batavia (1998); at CBPF, Rio de Janeiro (2000) and at Vietri, Italy (2002). For the 2002 edition, it was decided to widen the conference target, renaming it "Heavy Quarks and Leptons".

The 2004 edition will be held in San Juan, Puerto Rico, on June 1-5. The University of Puerto Rico at Mayaguez is the host institution and Dr. Angel Lopez is the Conference Chairman. Other members of the UPR HEP group are serving on the local organizing committee.

A distinguished group which comprises the International Advisory Committee is helping Dr. Lopez organize the technical sessions of the conference.

Members of the HQL2004 International Advisory Committee

- Ikaros Bigi
- Brad Cox
- Stephan Paul
- Stefano Bianco

- Konrad Kleinknecht
- Giancarlo DAmbrosio
- Franco L. Fabbri
- Alberto Reis
- Gianpaolo Bellini
- Joel Butler
- Peter Dornan
- Vera Luth
- Hitoshi Yamamoto
- Ritchie Patterson
- Adam Para
- Franco Grancagnolo

The preliminary schedule calls for a total of 28 hours of plenary talks. Table lists the main topics to be covered. More information can be found at the conference website http://charma.uprm.edu/hql04.

Based on past conferences in this series, attendance of some 70 participants is expected. Since all talks are plenary talks, a poster session is planned to allow a larger participation specially by young physicists. There will also be a prize for the best participation by a young physicist.

This proposal is requesting funds to help defray some of the costs associated with the conference. The conference proceedings will be published.

Old San Juan will make for a stimulating setting for HQL2004. This will be a very active year for heavy quark physics with many new results from the collider experiments that are presently running, with the excitement of the start of CLEOc data acquisition and the plans for a rich program at the second generation proton collider B experiments. It should all make for a most special conference.

Conference Topics

- Production and Spectroscopy
- Heavy Quark Decays
- CP Violation and Mixing
- D and B Rare Decays
- Kaon and Hyperon Decays
- Lepton Decays
- Neutrino Oscillations

Bibliography

[1] L. Wolfenstein *Phys. Rev. Lett.*, vol. 51, p. 1945, 1983.

[2] J. M. Link *et al.*, "New measurements of the D^0 and D^+ lifetimes," *Phys. Lett.*, vol. B537, pp. 192–200, 2002.

[3] K. Hagiwara *et al.*, "Review of particle physics," *Phys. Rev.*, vol. D66, p. 010001, 2002.

[4] B. Guberina, S. Nussinov, R. D. Peccei, and R. Ruckl, "D meson lifetimes and decays," *Phys. Lett.*, vol. B89, p. 111, 1979.

[5] B. Guberina, R. Ruckl, and J. Trampetic, "Charmed baryon lifetime differences," *Z. Phys.*, vol. C33, pp. 297–305, 1986.

[6] G. Bellini, I. I. Y. Bigi, and P. J. Dornan, "Lifetimes of charm and beauty hadrons," *Phys. Rept.*, vol. 289, pp. 1–155, 1997.

[7] B. Guberina and B. Melic, "Inclusive charmed baryon decays and lifetimes," *Eur. Phys. J.*, vol. C2, p. 697, 1998.

[8] I. I. Y. Bigi, "Heavy quark expansions for inclusive heavy-flavour decays and the lifetimes of charm and beauty hadrons," 1996. Talk given at Workshop on Heavy Quarks at Fixed Target (HQ 96), St. Goar, Germany, 3-6 Oct 1996 (UND-HEP-96-BIG06).

[9] B. Blok and M. A. Shifman, "Lifetimes of charmed hadrons revisited. facts and fancy," 1991. Talk given at 3rd Workshop on the Tau-Charm Factory, Marbella, Spain, 1-6 Jun 1993 (TPI-MINN-93-55-T, UMN-TH-1227-93, TECHNION-PH-93-41).

[10] H.-Y. Cheng, "A phenomenological analysis of heavy hadron lifetimes," *Phys. Rev.*, vol. D56, pp. 2783–2798, 1997.

[11] J. M. Link *et al.*, "A high statistics measurement of the Λ_c^+ lifetime," *Phys. Rev. Lett.*, vol. 88, p. 161801, 2002.

[12] J. E. Ramirez, "Lifetime measurement of the charmed strange baryon Ξ_c^+," 2002. FERMILAB-THESIS-2002-24.

[13] J. M. Link *et al.*, "A new measurement of the Ξ_c^+ lifetime," *Phys. Lett.*, vol. B523, pp. 53–59, 2001.

[14] A. H. Mahmood *et al.*, "Measurement of the Ξ_c^+ lifetime," *Phys. Rev.*, vol. D65, p. 031102, 2002.

[15] J. Rademacker, "Heavy flavour lifetimes and lifetime differences," *ECONF*, vol. C0304052, p. WG114, 2003.

[16] P. Abreu *et al.*, "Measurement of the lifetime of b-baryons," *Eur. Phys. J.*, vol. C10, pp. 185–199, 1999.

[17] K. Anikeev *et al.*, "B physics at the tevatron: Run ii and beyond," 2001.

[18] C. Tarantino, "Beauty hadron lifetimes and b-meson cp-violation parameters from lattice qcd," 2003. Invited talk at "International Europhysics Conference on High-Energy Physics" (HEP 2003), Aachen, Germany, 17-23 Jul 2003.

[19] W. A. Rolke and A. M. López, "Correcting the minimization bias in searches for small signals," *Nucl. Inst. Meth.*, vol. A503, pp. 617–624, 2003.

[20] R. D. Cousins and G. F. Feldman, "A unified approach to the classical statistical analysis of small signals," *Phys. Rev.*, vol. D57, p. 3873, 1998.

[21] W. A. Rolke and A. M. López, "Confidence intervals and upper bounds for small signals in the presence of background noise," *Nucl. Inst. Meth.*, vol. A458, pp. 745–758, 2001.

[22] C. Caso *et al.*, "Review of particle physics," *Eur. Phys. J.*, vol. C3, p. 177, 1998.

[23] W. A. Rolke and A. M. López, "Bias-corrected confidence intervals for rare searches," pp. 44–48, 2002. Proceedings of the Conference on Advanced Statistical Analysis and Technology.

[24] G. Feldman, "Multiple measurements and parameters in the unified approach," pp. 10–14, 2000. Talk at Fermilab Workshop on Confidence Limits 27-28 March, 2000, `http://conferences.fnal.gov/cl2k`.

[25] B. Efron, "Bootstrap methods: another look at the jackknife," *Ann. Statistics*, vol. 7, pp. 1–26, 1979.

[26] P. Hall, "The bootstrap and edgeworth expansion," *Springer Verlag*, 1992.

[27] K. G. Hayes, M. L. Perl, and B. Efron, "Application of the bootstrap statistical method to the tau decay mode problem," *Phys. Rev.*, vol. D39, p. 274, 1989.

[28] R. Alfieri *et al.*, "Understanding stochastic perturbation theory: toy models and statistical analysis," 2000.

[29] B. Efron and R. J. Tibshirani, "An introduction to the bootstrap," 1993.

[30] P. Frabetti *et al.*, "Description and performance of the fermilab e687 spectrometer," *Nucl. Inst. Meth.*, vol. A320, p. 519, 1992.

[31] P. Frabetti *et al.*, "A wideband photon beam at the fermilab tevatron to study heavy flavors," *Nucl. Inst. Meth.*, vol. A329, p. 62, 1993.

Appendix A

UPR Contributions to BTeV

UPR Past Contributions to BTeV

As detailed in the BTeV Preliminary Technical Design Report of 1999, MCFast simulations of the dimuon triggering performance suggested that rejection ratios of 500-600 for minimum bias events could be achieved with an efficiency of roughly 95% of the geometrical acceptance (18% total efficiency) for $B^0 \rightarrow J/\psi K_s^0$ where the J/ψ decays to two muons. However, a more realistic simulation was necessary to study the viability of a dimuon trigger.

By December 1999 the BTeV simulation group had developed the foundations for a GEANT simulation. They had also developed modules for the main tracking detectors, the pixels and straw tubes. The UPR group (Xiong and Lopez) added a muon detector module to this foundation. The pie-wedge octagonal geometry of the sensor planes in each arm of the detector were defined. If one takes the term "plane" to mean one layer of the double layers in the planks, there is a total of thirty six planes considering that half the octants in one station are at a different longitudinal position than the other half in order to permit overlap at the octant borders. (This geometry included only three views per station instead of four as in the proposal.) The size and magnetic fields of the filters and all positions of the sensor planes were included in detail. All default processes in GEANT were simulated in addition to δ-rays. Photons and electrons were traced down to an energy of 0.1 MeV while hadrons and muons were traced down to 10 MeV. The information that was recorded included the type, momentum and parent of each particle which left a hit in the muon system as well as a list of all hits associated with the particle.

Figure A.1 presents the results on the characteristics of the hits in the muon detector for $B^0 \rightarrow J/\psi K_s^0$ events where the average number of interactions (minimum bias) per crossing has been taken as two. Most of the hits in the detector are not due to muons but are due to low momentum secondaries coming from interactions with the walls of the beam hole in the muon filters as is evident from the radial position distributions at the downstream faces of the filters. Secondaries spray out of the downstream ends of the holes in both filters. Figure A.2a documents this problem. The hit distribution in the muon planes can be understood by considering that the percentage of such tracks striking a given plane will increase with the lever arm between the nearest filter and the plane. (All planes go down to the same radial position.) The effect is noticeable in stations 1 and 2 which are just downstream of filters but is largest for station 3. All planes in station 3 receive a large flux due to the long lever arm between this station and the second filter.

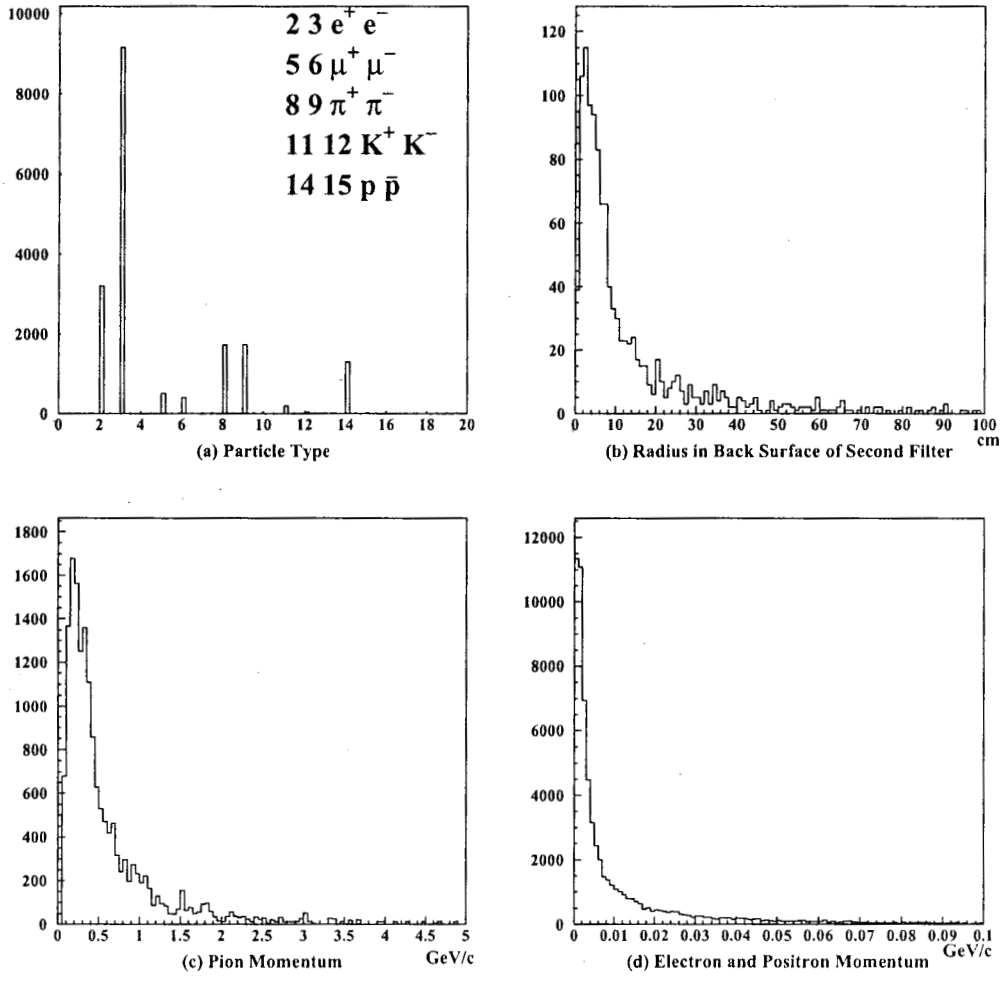

Figure A.1: Characteristics of muon detector hits for $J/\psi\, K_s^0$ events. (a) Particle type. Each particle type is assigned an integer code, shown in the legend. For example, π^+ is given the code 8. The electromagnetic and hadronic noise is larger than the muon signal. The excess of electrons over positrons is due to δ-ray production. (b) Projected radial position at the downstream face of the second filter for tracks that hit station 3. The large percentage of tracks emanating from the vicinity of the hole in the filter is quite evident. (c) and (d) Momentum of pion and e^+/e^- noise. Noise secondaries have much lower momentum than J/ψ muons.

To reduce the noise hit level in the third station, Xiong and Lopez suggested the addition of a 30cm thick shielding block just in front of that station. This suggestion was included in the design and the improved distributions are presented in A.2b. The choice of the shielding block thickness was based on a study whose results are presented in (Fig. A.3). Interactions with the beam pipe as well as δ-ray production also contribute significantly to the noise. Xiong and Lopez also suggested adding

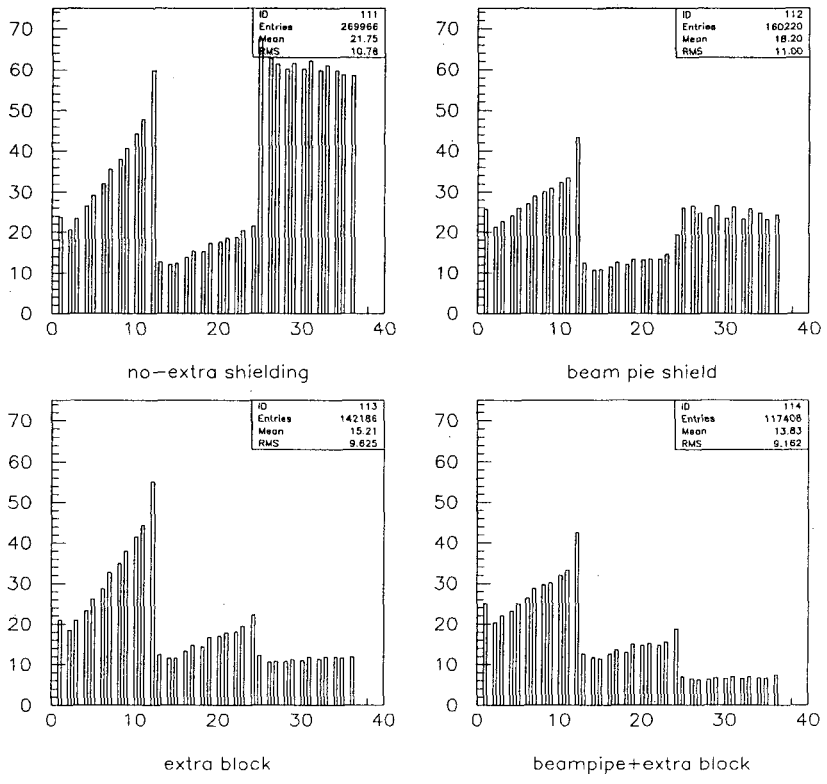

Figure A.2: Distribution of hits among muon detector planes for different shielding configurations. There are twelve planes per station. (a: upper left) Original design; no extra shielding. (b: lower left) Extra shielding block in front of the third station. (c: Upper right) Extra shielding around the beam pipe. (d: Lower right) Both beam pipe and third station shielded.

shielding around the beam pipe with the resultant improvement shown in Fig A.2c and A.2d. This was alsoincorporated into the baseline design.

It took an average of 10 minutes of CPU time in one of our Alpha OSF workstations to generate one GEANT event. However, by dedicating half of our workstation cluster to the task for one month, we were able to generate approximately 50,000 minimum bias events and 5,000 B to J/ψ signal events without unduly interrupting the rest of our analysis tasks.

The simulation data generated in Puerto Rico was added to a similar sample generated at Vanderbilt University and the total sample was used to study alternative trigger algorithms. We worked in collaboration with the University of Illinois and Vanderbilt on this task. All triggers modeled used only the information from the muon detector (stand-alone trigger). The "upper limit" on muon trigger performance was defined by a "tracking" trigger algorithm. This trigger loops over all hits within a given octant sector to choose the set of hits which has the lowest χ^2 for the hypothesis that the hits came from a track which emanated at the nominal beam center. A simplified magnetic description is

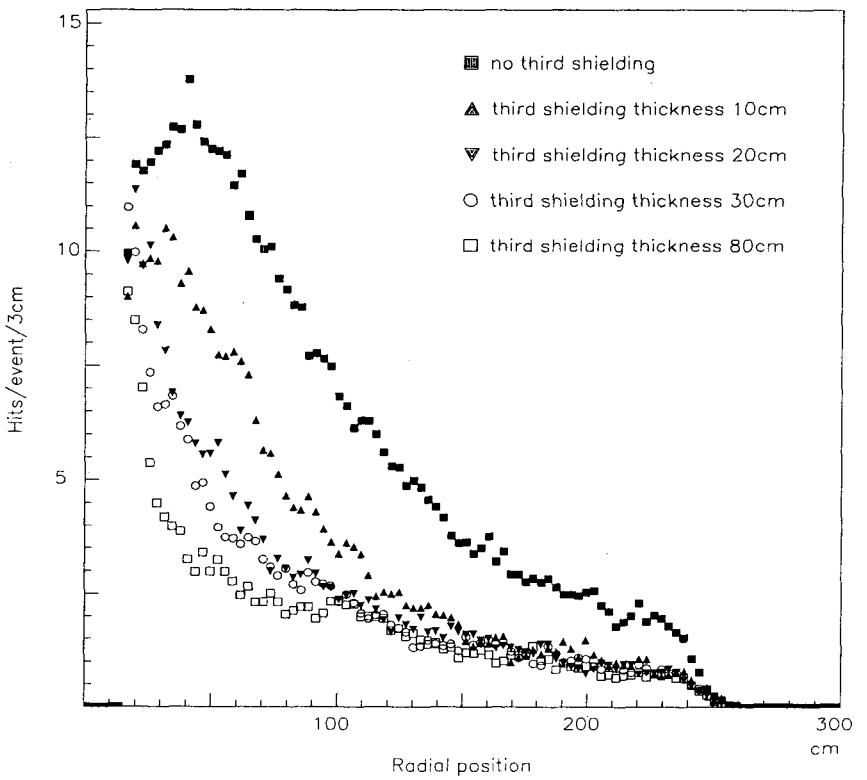

Figure A.3: The radial position of hits in the third station. Each symbol corresponds to a different shielding block thickness.

used in calculating the χ^2, correlations between planes and dE/dx losses are ignored and all equations are linearized in the three fit parameters which are 1/p and the slopes of the track at the origin. A miminum pre-trigger requirement was established as having two "muons" ($\chi^2 < 25.2$) of opposite charge in two different octants. Trigger efficiency and rejection power were studied as a function of cuts on the χ^2 and transverse momentum of the candidate muons as well as on the minimum radius of all muon hits. Rejection ratios of 500 to 1 with simultaneous relative efficiencies of 50% were achieved with this trigger. (The relative efficiency was defined relative to J/ψ events where both muons have momentum greater than 5 GeV and leave hits in all three muon stations.) The GEANT simulation is much more realistic than MCFast. The average occupancy with GEANT (1.2% for minimum bias events) is 100 times larger than with MCFast; nevertheless, the "tracking trigger" should provide satisfactory performance. In particular it will use only a small fraction of the Level-1 bandwidth which is dominated by the vertex trigger which rejects at 100 to 1. Since it is "stand-alone", the dimuon trigger can be used to calibrate the vertex trigger.

As to the muon detector hardware, by 1999 the preliminary design became detailed enough that prototype units of the component proportional tube planks could be built at Vanderbilt University. These planks consisted of a double layer of 32 tubes with common end caps which serve as a gas

manifold and a base for the electrical connections. The front end electronics were mounted on circuit boards which plug into sockets on the end cap. Prototypes of these circuit boards were also built.

The UPR participated in a beam test of ten of these prototype planks which was carried out at Fermilab's meson area in the summer of 1999. Besides working on the assembly of the test system (Lopez and Xiong), the UPR group developed routines to find tracks using the hits in the tubes and took shifts during the data runs (Xiong).

The main result from these beam tests was that the basic design was sound but that additional RF shielding was needed for the electronics. ASD8B chips (developed at the University of Pennsylvania) were used to amplify and digitize the signals. It was found that these required a nearly complete Faraday cage to lower RF noise to acceptable levels. This finding has led to changes in the design. We are now planning to solder the tubes to a brass gas manifold instead of gluing them to a manifold made of an insulator material as in the prototype. The tubes and manifold will be electrically connected to aluminum sheets which will extend out to the end of the electronics forming a Faraday cage around the electronics. For the prototype test, makeshift Faraday cages were built from Aluminum foil and the amplifier cards were placed in boxes made of copper plated G10. With such a scheme, noise was reduced to acceptable levels and the gain of the ASD8B was found to be sufficient. (In the actual detector we plan to use the improved version (ASDQ)).

Another problem uncovered by the beam test was cross-talk between channels. Instead of having one or two tubes fire per particle crossing, sometimes there would be five or six. This problem was alleviated by adding termination resistors to the open end of the tubes. Although such resistors will lower the gain by a factor of two, our tests show that there will be more than enough gain to be able to use them. Additional changes are planned to the front-end electronics.

Appendix B

Analysis of the BTeV Muon Trigger Design

DRAFT of BTeV Internal Memo

Zhongchao Li - Angel Lopez
Univ. of Puerto Rico at Mayaguez
October, 2003

DRAFT of BTeV Internal Memo

Abstract

DRAFT of BTeV Internal Memo

Instead of deriving parameter values from fitting to Monte Carlo data, in this note we show that the "track" and "charge" equations in the muon trigger algorithm can be deduced analytically solely from the muon detector geometry parameters. We also find that the momentum of the muon track can be easily obtained. This suggests that the equations can be used for pattern recognition in reconstruction. Furthermore, we derived similar equations for the hits in the u and v views. The formula to discriminate left and right in the same octant is given with u and v hit information. Our conclusions were checked by using Monte Carlo data. Finally, based on our results, we give suggestions on the BTeV muon trigger scheme.

B.1 Introduction

DRAFT of BTeV Internal Memo

The current BTeV muon trigger design is based on analyzing muon Monte Carlo data, as shown in figure B.1. The blue dots in left plot of figure B.1 are the r-space coordinates of good muon tracks. These points lie in a very well defined plane as shown in right plot of figure B.1. The "track equation" of this plane can be found using a simple linear fit to the blue (good muon) points, i.e.

$$R_2 = 27.69 - 1.26R_0 + 2.20R_1 \tag{B.1}$$

where R_0,R_1,R_2 is the number of the proportional tube hit by the muon in stations 0,1,2. Note that the tubes are numbered from outside in: tube 0 is the outermost and tube 383 is the innermost in each view.

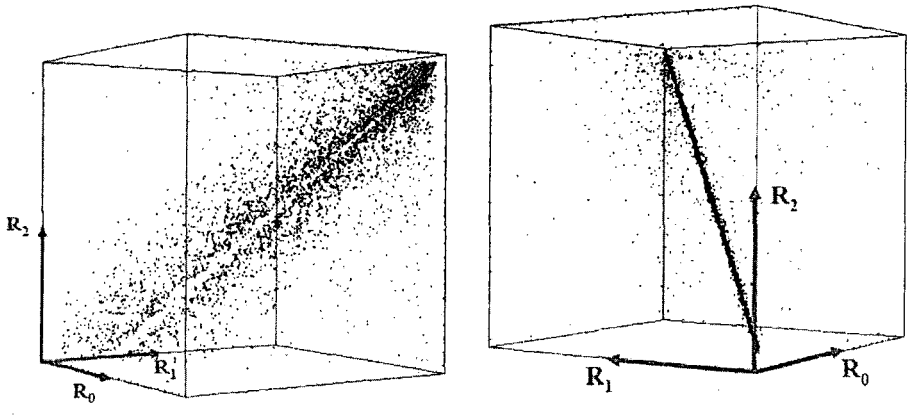

Figure B.1: Left plot: Plot of (R_0,R_1,R_2) for each of 2200 good muon tracks (blue dots) and the closest (R_0,R_1,R_2) co-ordinate for each of 4300 minimum bias events (red dots). Right plot: the left plot has been rotated to illustrate that all of the good muon tracks (blue dots) result in (R_0,R_1,R_2) coordinates that lie on a well defined plane.

Another interesting fact that is "observed" in the Monte Carlo data is that the charge separation is very clear, and indeed, nearly perfect charge identification can be obtained by considering only the (R_0,R_2) projection of this plane (shown as figure B.2). The "charge equation" is:

$$R_2 = 1.275R_0 - 125 \tag{B.2}$$

For details, please refer to Mats Selen's document [1] and presentation [2].

Instead of this kind of "empirical" approach, in this note, we first show that the equations B.1, B.2 can be deduced analytically solely from the muon detector geometry parameters. Secondly, the momentum formulae including the "charge equation" can be obtained naturally. Thirdly, we get the relationships of hits in all views using the same general approach. The formula to discriminate left and right in the same octant is given with U, V hit information. All of these results were checked with the Monte Carlo data. Finally, we make suggestions on the BTeV muon trigger scheme.

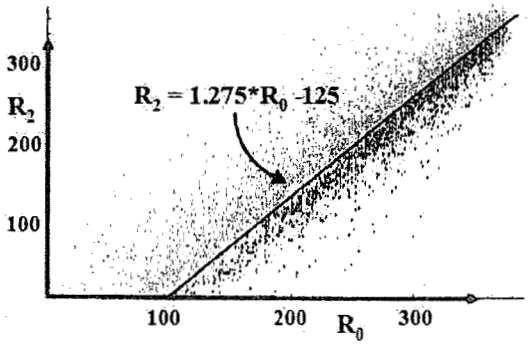

Figure B.2: Plot of R_2 vs R_0 for each of 1100 positive muon tracks (purple points) and 1100 negative muon tracks (green points). The blue line is a fit to the "gap" between positive and negative tracks.

B.2 Deduction of equations analytically

B.2.1 Deduction of "track equation"

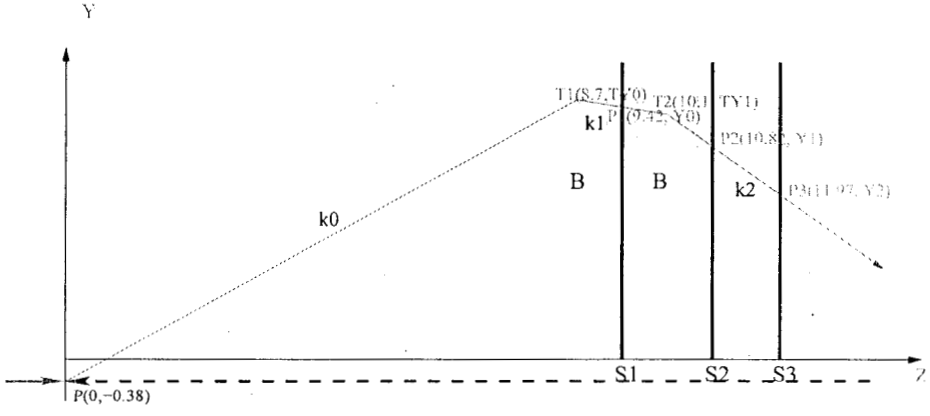

Figure B.3: Muon Propagation in Muon Detector

Following the description of the muon detector in the BTeV proposal [3], we define the reference frame as: Z axis is the beam direction, Y axis is the center of r view. The figure B.3 is the projection of one track in YZ plane. Assuming the dipole magnetic field in the inner detector can be ignored, a muon track originates from the interaction region P(0,-0.38), then it propagates through three stations S1, S2, S3 and leaves hits at P1(9.42, Y0), P2(10.82, Y1), P3(11.97, Y2). To simplify the problem, the track is supposed to be "kicked" at the center of the toroids at T1(8.7, TY0) and T2(10.1, TY1), as shown in figure B.3.

The muon momentum can be determined by the deflection angle in the toroidal magnetic field. In other words, the signed momentum can be expressed approximately:

$$p = \frac{B}{(k_2 - k_1) \times cos\theta}, \; B = \int B(x,y)\, dz = 1.5 \;\; T \cdot m \tag{B.3}$$

Where B is the integrated magnetic field and should be a constant, k_1, k_2 is the slope before and after the second "kick" in YZ plane. And θ is the angle from the center of r view to an arbitrary hit in r view, refering to figure B.7. Its range is from $-22.5°$ to $22.5°$.

In the following lines, we are trying to get the k_0, k_1, k_2. Firstly, get the linear equation of line p_2p_3:

$$\begin{aligned} Y &= k_2 Z + b_2 \\ k_2 &= \frac{Y_2 - Y_1}{11.97 - 10.82} = \frac{Y_2 - Y_1}{1.15} \\ b_2 &= Y_2 - 11.97\frac{Y_2 - Y_1}{1.15} = -\frac{10.82}{1.15}Y_2 + \frac{11.97}{1.15}Y_1 \\ TY_1 &= 10.1 \times k_2 + b_2 = -\frac{0.72}{1.15}Y_2 + \frac{1.87}{1.15}Y_1 \end{aligned} \tag{B.4}$$

For line p_1p_2:

$$\begin{aligned} k_1 &= \frac{TY_1 - Y_0}{10.1 - 9.42} = \frac{-\frac{0.72}{1.15}Y_2 + \frac{1.87}{1.15}Y_1 - Y_0}{0.68} \\ &= -\frac{0.72}{1.15 \times 0.68}Y_2 + \frac{1.87}{1.15 \times 0.68}Y_1 - \frac{1}{0.68}Y_0 \\ b_1 &= Y_0 - 9.42 \times k_1 = \frac{0.72 \times 9.42}{1.15 \times 0.68}Y_2 - \frac{1.87 \times 9.42}{1.15 \times 0.68}Y_1 + \frac{10.1}{0.68}Y_0 \\ TY_0 &= 8.7k_2 + b_2 = \frac{0.72 \times 0.72}{1.15 \times 0.68}Y_2 - \frac{1.87 \times 0.72}{1.15 \times 0.68}Y_1 + \frac{1.4}{0.68}Y_0 \end{aligned} \tag{B.5}$$

For line pp_2:

$$k_0 = \frac{TY_0 + 0.38}{8.7} = \frac{0.72 \times 0.72}{1.15 \times 0.68 \times 8.7}Y_2 - \frac{1.87 \times 0.72}{1.15 \times 0.68 \times 8.7}Y_1 + \frac{1.4}{0.68 \times 8.7}Y_0 + \frac{0.38}{8.7} \tag{B.6}$$

Supposing energy loss of charged particle(e, π, μ) can be expressed $f(id, p)$, where p is the momentum. According to equation B.3:

$$\frac{1}{k_1 - k_0} = f(id, p)\frac{1}{k_2 - k_1}, 0 < f(id, p) \leq 1. \tag{B.7}$$

As for the high energy muon, supposing $f(\mu, p) = 1$. Then equation B.7 can be:

$$k_2 + k_0 - 2k_1 = 0 \tag{B.8}$$

Replace k_2, k_1, k_0 in equation B.8 with equation B.4, B.5, B.6 and we get:

$$\begin{aligned} &\left(\frac{1}{1.15} + \frac{0.72 \times 0.72}{1.15 \times 0.68 \times 8.7} + \frac{2 \times 0.72}{1.15 \times 0.68}\right) Y_2 \\ &- \left(\frac{1}{1.15} + \frac{1.87 \times 0.72}{1.15 \times 0.68 \times 8.7} + \frac{2 \times 1.87}{1.15 \times 0.68}\right) Y_1 \\ &+ \left(\frac{1.4}{0.68 \times 8.7} + \frac{2}{0.68}\right) Y_0 + \frac{0.38}{8.7} = 0 \end{aligned}$$

$$2.7872Y_2 - 5.8501Y_1 + 3.1778Y_0 + \frac{0.38}{8.7} = 0 \tag{B.9}$$

Note that in equation B.9, Y_2, Y_1, Y_0 is the coordinate with the units meter. Now we are going to transform them into tube numbers R_2, R_1, R_0, i.e.

$$Y = (384 - R) \times \frac{2.4 - 0.38}{384} = (384 - R) \times 0.00526 \tag{B.10}$$

Then equation B.9 can be written:

$$2.7872\,(384 - R_2) - 5.8501\,(384 - R_1) + 3.1778\,(384 - R_0) + \frac{0.38}{8.7 \times 0.00526} = 0$$

At last, we got the "track equation":

$$R_2 = 18.82 - 1.14R_0 + 2.10R_1 \Rightarrow -R_2 + 2.10R_1 - 1.14R_0 + 18.82 = 0 \tag{B.11}$$

Now, let's check this result with Monte Carlo data. We select the good muons with program, and retrieve the track information, including hit tubes, the momentum. Figure B.4(a) show the equation B.11 is really a good description of the good muon hits in r view. As for the smeared distribution is due to the muon's multi-scatter and the deflection by the inner magnetism. Comparing Figure B.4(a) with (b), they are similar.

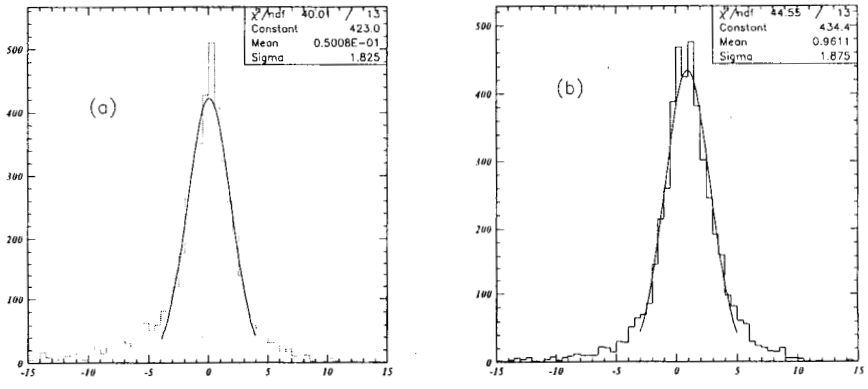

Figure B.4: (a)Eq. $-R_2 + 2.10R_1 - 1.14R_0 + 18.82 = 0$ (b)Eq. $-R_2 + 2.20R_1 - 1.26R_0 + 27.69 = 0$

And now it is clear that why this equation can be used to select the good muon. Refer to eq. B.7, for minus events, the energy loss coefficients $f(e,p)$, $f(\pi,p)$ or k_0 are different to that for good muons, so their "track equation" will be different either.

Even with a few simplification, we got almost the similar equation with the equation B.1 which was got by fitting. However, the relative bigger difference in constants(18.82 vs. 27.69) is due to the removal of dipole magnetism in our calculation.

With the similar way, we can deduce the track eauation for u,v,s views from eq. B.9.

$$-U_2 + 2.10U_1 - 1.14U_0 + 18.82 = 0$$
$$-V_2 + 2.10V_1 - 1.14V_0 + 18.82 = 0$$
$$-S_2 + 2.10S_1 - 1.14S_0 + 18.82 = 0$$

B.2.2 The "charge equation" and muon momentum

Now, we are going to get the signed momentum according to eq. B.3.

$$\begin{aligned} k_2 - k_1 &= \frac{0.68 + 0.72}{1.15 \times 0.68} Y_2 - \frac{0.68 + 1.87}{1.15 \times 0.68} Y_1 + \frac{1}{0.68} Y_0 \\ &= [1.7903\,(384 - R_2) - 3.2609\,(384 - R_1) + 1.4706\,(384 - R_0)] \times 0.00526 \\ &= (-1.7903R_2 + 3.2609R_1 - 1.4706R_0) \times 0.00526 \end{aligned} \quad \text{(B.12)}$$

Since a good muon track must satisfied eq. B.11, R_1 can be substituted by R_2 and R_0.

$$k_2 - k_1 = (-R_2 + 1.2707R_0 - 123.504) \times 0.00526 \quad \text{(B.13)}$$

$$p = \frac{B}{(k_2 - k_1) \times cos\theta} \Rightarrow p \cdot \cos\theta \cdot (-R_2 + 1.2707R_0 - 123.504) \times 0.00526 = B \quad \text{(B.14)}$$

From r view, it is impossible to know the θ, but the range of $cos\theta$ from 0.924 to 1. Refer to formula B.19, we got $cos\theta$:

$$cos\theta = cos[atan\frac{(U_1 - V_1)/(2 \cdot sin22.5°)}{(384 - R_1) + 0.38/0.00526}]$$

From plot B.5(a), the integrated magnetic field is about 1.5. And the charge of the muon can be determined from eq. B.13 by the sign of momentum, Please refer to B.5(b). Then the "charge equation" can be deduced, i.e.

$$R_2 = 1.2707R_0 - 123.504 \quad \text{(B.15)}$$

This is almost same with eq. B.2.

Figure B.5(b) show the reconstructed muon momentum versus Monte Carlo generated momentum. The error is big because the spatial resolution is 1 tube width.

However, for dimuon for J/Psi, the sum of two signed momentum(this mean difference of momentum between dimuons) should be small no matter the momentum of muons. Refer to left plot figure B.6. Right plot in figure B.6 is comparison with the Monte Carlo momentum. This seem not to be a effective cut.

And eq. B.9 should be effective in the pattern recognition of muon track during event reconstruction because the hit position(Y_2, Y_1, Y_0) can be obtained precisely by r view, s view or u and v view individually. No Monte Carlo data at persent is availble to study this.

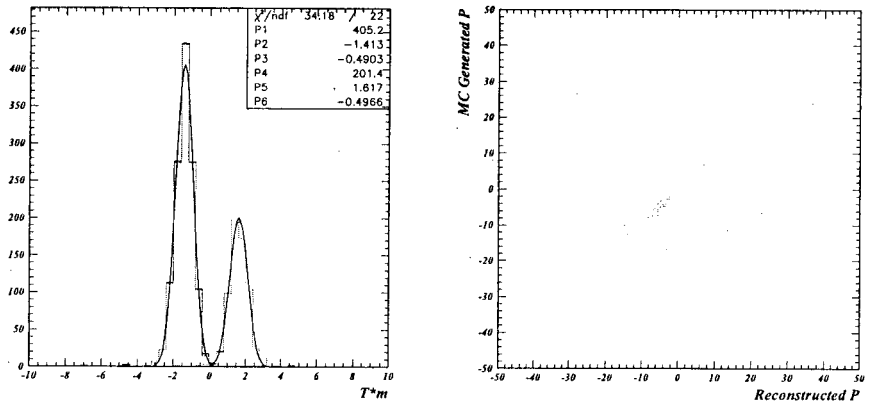

Figure B.5: (a)The blue line is minus muon event from MC, there is only few events with wrong sign. Same for plus muon. That mean almost perfect charge determination. (b)Reconstructed muon momentum versus Monte Carlo generated momentum

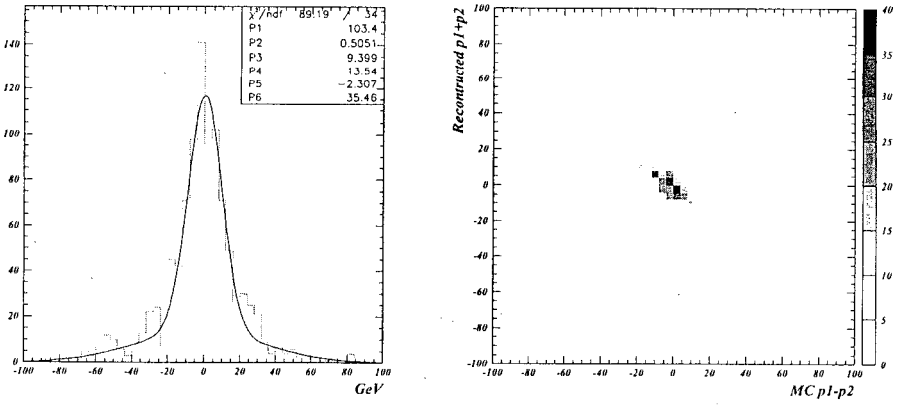

Figure B.6: Difference of momentum between dimuons from psi

B.3 r, u, v relationship and left-right discrimination

The plank dimensions for the standard geometry [4] is shown as in table B.1.

Plank	outerrad	r-views length	u/v-view length
0	239.999527	200.822128	68.8713379
1	223.174561	186.883865	109.490402
2	206.349609	172.945618	150.109421
3	189.524643	159.007355	187.094376
4	172.699677	145.069092	174.699677
5	155.874725	131.130859	157.874725
6	139.049759	117.192596	141.049759
7	122.224800	103.254341	124.224800
8	105.399841	89.3160858	107.399841
9	88.5748825	75.3778381	90.5748825
10	71.7499237	61.4395828	73.7499237
11	54.9249573	47.5013237	56.9249573

Table B.1: Plank Dimensions. Planks are numbered from the outside in. The outer edge of the plank and the length are given. The outer edge is measured by drawing a line perpendicular to the planks. For the r-view this goes through the center of the plank and for the u and v views this line goes along one edge.

According to the dimensions, we figured out the diagrams of it. Please refer to figure B.7. Following, we are going to deduce the relationships. Supposing a muon hit r,u,v views vertically in point A(R,U,V), as shown in the figure B.7. Vector from center of r-view to A is $\vec{X}$. R_u and R_v are the U and V's interception with the center of r-view. From right-angle triangles $\triangle CDR_u$ and $\triangle CER_v$ in the figure, it is easy to figure out:

$$U = (R_u + K) \cdot cos22.5^\circ \tag{B.16}$$

$$V = (R_v + K) \cdot cos22.5^\circ \tag{B.17}$$

where R_u, R_v, U, V, K are hit tube numbers. we measured the distance from B to C, which is about 0.19m. Then the K is:

$$K = \frac{0.19}{0.00526} = 36.12$$

Let us add equation B.16 with B.17, we got

$$U + V = (R_u + R_v + 2K) \cdot cos22.5^\circ$$

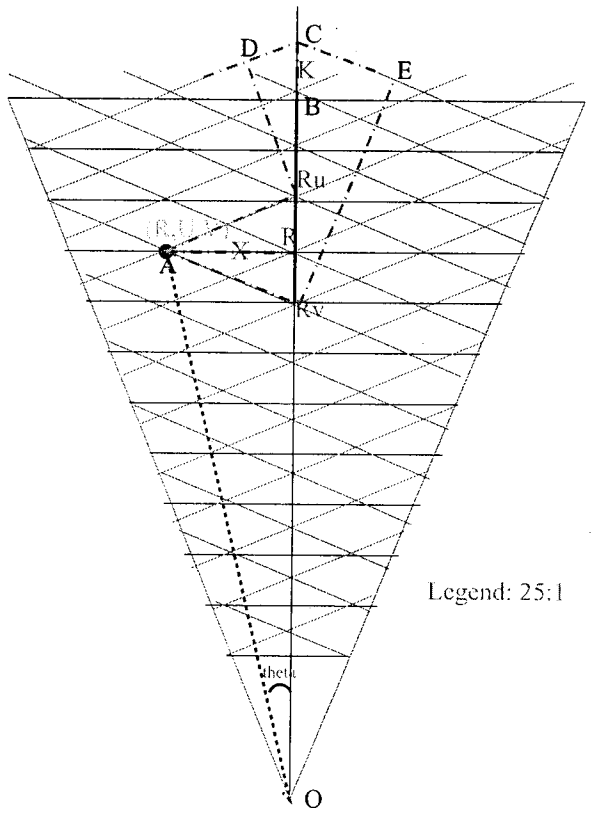

Figure B.7: Standard Geometry and ruv relationship

From triangle $\triangle ARR_u$ and $\triangle ARR_v$, we know $R - R_u = R_v - R$, i.e. $R_u + R_v = 2R$. Then equation B.18 is:

$$U + V = 2(R + K) \cdot cos22.5^\circ \Rightarrow U + V - 2R \cdot cos22.5^\circ = 66.75$$

This is r,u,v relationship that Mats Sellen call it as "spacepoint". However he get the K from Monte Carlo data. Figure B.8 is the MC data. In real situation, the track is not perpendicular to r,u,v views, so the distribution is smeared.

Since this relationship only come from the geometry, it can remove randomly noise. If one charged particle hit r view, it can hit u,v and s view too.

Now subtracting equation B.16 to B.17, we got:

$$U - V = (R_u - R_v) \cdot cos22.5^\circ \tag{B.18}$$

In triangle $\triangle AR_uR_v$, we know

$$\vec{X} = \frac{R_u - R}{tan22.5^\circ} = \frac{R_u - R_v}{2 \cdot tan22.5^\circ}$$

Then substitue eq. B.18 in $\vec{X}$.

$$\vec{X} = \frac{U - V}{cos22.5^\circ \cdot tan22.5^\circ \cdot 2} = \frac{U - V}{2 \cdot sin22.5^\circ}$$

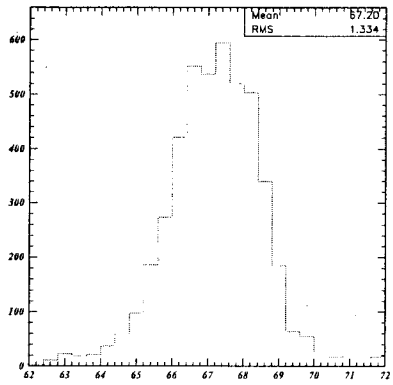

Figure B.8: r,u,v relationship

Note that $\vec{X}$,U,V are tube number. To transform into meters, then

$$\vec{X} = \frac{U-V}{2 \cdot sin22.5^\circ} \times 0.00526, \qquad \begin{cases} left\ side & U-V < 0 \\ right\ side & U-V \geq 0 \end{cases}$$

We ploted the distance to the center of r view as below in firgure B.9(a).
In the same way, refering to figure B.9(b), the distance to center of r view for u and v views is:

$$\vec{X} = \frac{U-V}{sin45^\circ} \times 0.00526$$

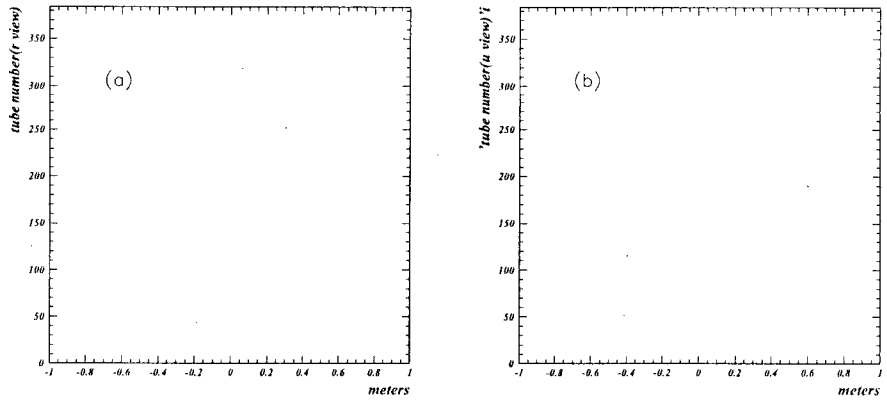

Figure B.9: r and u view

Then the $tan\theta$ in any station should be:

$$tan(\theta) = \frac{\vec{X}}{(384-R) \cdot 0.00526 + 0.38} = \frac{(U-V)/(2 \cdot sin22.5^\circ)}{(384-R) + 0.38/0.00526}$$

B.4 Suggestion on the trigger design

The current 3/4 scheme [1] only use the "track eqatuions", it looks fine from our MC data. However, it is lack of flexibility, we think, to possible change during running. For example, the unforeseeable detector problems, the difference of real background in real running and that in the Monte Carlo data, etc. So we suggest to study schemes with "spacepoint". Then the trigger can be fulfilled with two independent modules.

module 1/2(rs, uv) In each octant, we look for tracks in four views. A track is defined as at least one of r,s views and at least one of u,v views passing the distance cut to track plane. We call it module 1/2(rs,uv). This can improve the trigger efficiency when single tube's efficiency is bad or one view in octant is broken. For example, supposing single wire efficiency is 90%, then with 3/4 scheme, trigger efficiency should be 94.77%. With this scheme, it should be 98.01%.

module 2/3(ruv, suv) A good track require at least two of ruv spacepoints and at least two of suv spacepoints in three stations in the same octant. Why two? Just in order to let the trigger efficiency higher in case low single tube efficiency.

In both module, the parameters can be programmable in hardware.

The two schemes can be figured out.

a) Find the spacepoint and then look for tracks.

b) Find the tracks and then look for spacepoints.

The trigger efficiency for scheme a and b seem to be almost same. however the rejection ratio and the consumed time for hardware maybe very different. With these schemes, we expect the trigger efficiency should like that of 2/4 views in Mats's scheme. And the rejection should like that of 3/4 views scheme [1].

We can use Monte Carlo data to check this idea and check if they can be implemented in hardware.

Bibliography

[1] Mats Selen, *Muon Trigger System Supporting Documentation*, BTeV document 1167.

[2] Mats Selen, *The BTeV Muon Trigger*, BTeV document 1222.

[3] BTeV Collaboration, *BTeV Proposal*, BTeV document 316.

[4] Kevin Stenson, `http://www.hep.vanderbilt.edu/~stenson/btev/vampire.html`

Appendix C

Early UPR Contributions to FOCUS

C.1 Background on FOCUS Spectrometer

A detailed description of the E687 (FOCUS predecessor) beam and spectrometer can be found elsewhere [30, 31]. The two-magnet spectrometer identified charged and neutral hadrons, muons, electrons and photons. Charged particle tracking was accomplished by a silicon microstrip detector and a proportional chamber system. Three multi-celled Cerenkov counters provided charged particle identification. Neutral vees were reconstructed over a decay path of about 10 meters. Photons and electrons were detected by two lead/scintillator arrays, one at the center of the aperture and one at large angles. Muons were detected over the full aperture by scintillation hodoscopes and proportional tubes inserted behind steel hadron filters. A gas hadron calorimeter was used in the second-level trigger to reject purely electromagnetic events and increase the percentage of triggers containing charm (minimum hadronic energy requirement). This complement of detectors allowed the observation of a wide variety of charmed baryon and meson decay modes. In particular, the microstrip system separated tracks coming from the downstream decays of charmed particles from those coming from the primary production vertex.

The main goal of FOCUS was a tenfold increase in the number of charm events detected by an upgraded E687 spectrometer. This increase came from a factor of five increase in the beam flux and a factor of two improvement in efficiency. The increase in flux was due mainly to a change to liquid deuterium in the production target, the addition of a positron arm to the beam line and an increased primary proton flux. E687 and FOCUS' photon beam was created via the bremsstrahlung process from an electron beam (average energy 300 GeV in FOCUS) with a wide energy spread ($\pm 15\%$). This beam struck a lead (Pb) radiator (20% of a radiation length) to create the photon beam which had a similar energy spread around an average energy of 170 GeV.

The upgrades to the detectors for FOCUS (Fig. C.1) were directed mainly towards improving their capacity to handle the large increase in flux. Some detectors required only minor modifications but most underwent significant changes. Among these were the muon system, the hadron calorimeter, the inner electromagnetic calorimeter and the tracking system. The triggering strategy was changed to incorporate a new hadron calorimeter (scintillating tile design) in the first-level. The time response of the vertex microstrip detector and the muon system were significantly improved. A straw tube tracking

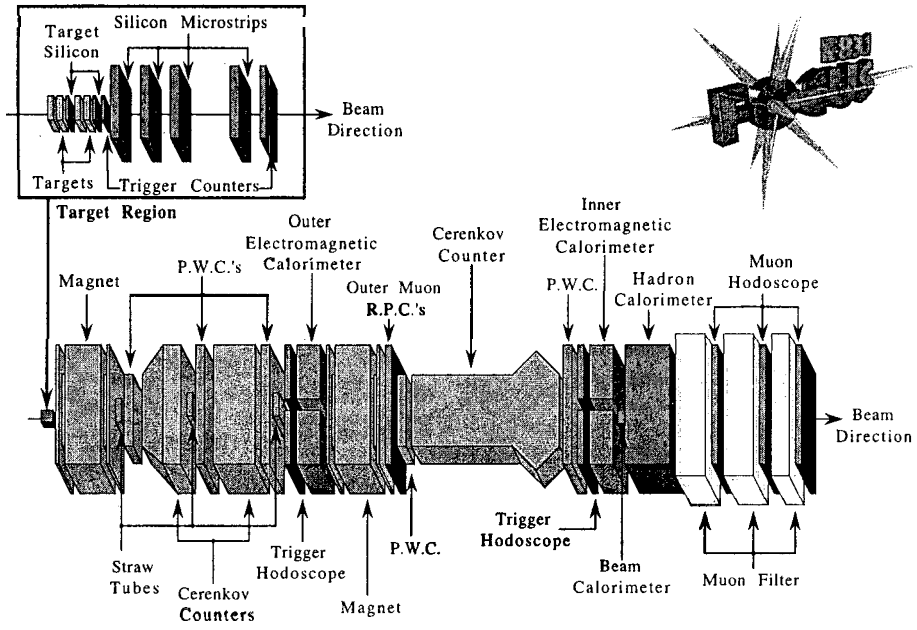

Figure C.1: Focus Spectrometer

system covered the beam region of the PWCs. The inner electromagnetic calorimeter was changed to a lead-glass array and the data acquisition system was completely rebuilt to handle the higher rates.

Major changes were implemented in the experimental target. Most of the data from E687 was obtained with a one-piece 4cm-long Be target. FOCUS used a segmented target of the same total length (but BeO) in order to increase the percentage of charm decay vertices occurring outside the material. This has been proven to significantly reduce backgrounds from secondary interactions in the target. Another important change in the target area was the addition of silicon planes interleaved with the target pieces. The "target silicon" planes improved the longitudinal position resolution of vertices from an initial $150\mu m$ down to $90\mu m$.

C.2 Contributions to FOCUS up to May, 2000

Our first FOCUS hardware responsibility concerned what we call the "inner" muon system which covered the central 40 mrad of the spectrometer. The E687 inner muon system consisted of 4 arrays of muon proportional tubes interspersed with coarse-granularity, triggering, scintillator arrays and hadronic filter steel. For FOCUS the proportional tubes were replaced with three scintillator counter hodoscopes (MH1-3). We were responsible for the design, construction, installation and commissioning of MH3. MH3 consisted of 108 counters arranged in two (U and V) stereo planes with their lengths aligned at 30^0 with respect to the X direction of the MH1 and MH2 arrays. The stereo angle significantly reduced our susceptibility to track matching confusion.

One of the areas in which FOCUS differed from E687 was the first level trigger. In E687, the dimuon trigger was at the second-level. In order to be able to take data at a higher beam intensity,

we needed to reduce the output rate of the first-level trigger in FOCUS. The hadronic energy trigger was brought to the first level for this purpose. If dimuon triggers were brought in at the second level, there would be an unnecessary hadronic energy threshold for each dimuon event. A completely new dimuon trigger system was designed and implemented by the UPR. A crucial aspect of the design was the use of high speed cables to meet the timing requirements. Their high cost forced us to place the logic electronics as close as possible to the detector minimizing the number of long cables runs. The IM trigger was one of the first triggers activated upon beam arrival. It was very useful in the commissioning of many detectors allowing calibration with minimum ionizing particles and the adjustment of the timing of channels with low flux.

FOCUS used the same Cerenkov system as E687 which consisted of three counters. UPR was responsible for two of these (C2 and C3) with a total of 210 channels. Besides repairing inoperative components, our group completely replaced the associated electronics with new ADCs and added TDCs to measure the signal timing for each channel. LED light sources were installed inside each counter and the high voltage for each channel was redetermined on the basis of the separation of the single-photoelectron signal peak from the ADC pedestal noise peak. Software developed by our group for this purpose was used for the adjustment of all the Cerenkov counters.

Dr. Mendez played a major role in the commissioning of the Outer Electromagnetic calorimeter and in the development of online and offline software. FOCUS greatly improved the electromagnetic particle detection and the ability to study channels with photon(s) in the final state. This improvement was accomplished by a "new" Inner (IE) and by an "upgraded" Outer (OE) calorimeters. The OE calorimeter (Frascati INFN) was composed of alternating layers of lead and scintillators strips and was upgrade by adding a new plane of square scintillator tiles covering showers in the small-angle, high occupancy region improving horizontal-vertical matching and cleaning π^0's peak by rejecting fake matches. The IE calorimeter (University of Colorado) was composed of lead glass blocks (802) arranged in a tower geometry. Both calorimeters had a vertical gap to allow the passage of the intense beam of non-interacting photons and e^+e^- from converted gammas. OE(IE) is located approximately at 900 cm (2600 cm) from the target and is sensitive to low (wide range) photon energies. The energy resolution for these calorimeters ($\sigma_E/E = a/\sqrt{E}$ where a $\approx$ 7% and 12% for IE and OE respectively) allow a good π^0 resolution and single photon isolation.

The FOCUS online software also was updated and in some cases completly re-written in response to the "new" implemented electronics (such was the case for the OE). Dr. Mendez and Dr. S. Bianco (a collaborator from Frascati) were in charge of the OE performance during the FOCUS run. Dr. Mendez developed the software to on-line monitor the calorimeter stability during the data taking period. The monitoring process included the ADC's pedestal read-out **during** (CONSUMER Program) and **between** (MONDA Program) beam spills. Because the electronics used by other detectors (IE and Cerenkov counters) in the experiment was common to the OE, this same software was used by the collaboration to minimize the hardware debugging time.

The laborious process of FOCUS data acquisition ended on September 1, 1997. The run was highly successful. The spectrometer suffered no major breakdowns and the UPR subsystems, in particular, had nearly perfect performance. The quality of the data from all detectors was monitored closely by performing a detailed analysis of a certain percentage of the data online. FOCUS wrote to tape approximately twelve times as many events as the totality of E687 with a similar charmed fraction and a superior data quality.

The UPR has also made significant contributions to the FOCUS software, both online and

offline: (1) a routine to unpack the muon detector data and make it accessible to the offline analysis package; (2) a complete inner muon identification package; (3) a set of routines to use the Cerenkov TDC information, (4) routines to simulate the performance of MH3 and the effect of pion punch-through in the muon detector, (5) routines to measure the efficiency of the HXV and OH trigger counters and to implement the use of precise, run-dependent efficiencies in the FOCUS simulation, (6) routines to use the data from other detectors to identify pions that decay in flight, and (7) routines to implement a selection algorithm for a secondary leptonic skim.

The development of the muon identification algorithm progressed from the measurement of the scintillator plane efficiency, through the measurement of the muon identification efficiency and the hadron misidentification rates, until the algorithm blossomed into a sophisticated tool which includes the capacity to diminish misidentification by eliminating the cases where a hadron is accompanied by a muon. The algorithm uses a continuous variable (a confidence level) as the identification criterion which provides added flexibility. The inner muon detector planes built by our group were found to be highly efficient. This together with the quality of the other muon planes and the high efficiency of the algorithm leads to muon identification efficiencies of 98% while **at the same time** proton misidentification levels are reduced to the level of 0.1% and pion misidentification (mostly due to decays in flight) are below 0.8% for most momenta. **The basic goals of the inner muon upgrade were achieved**. The FOCUS IM system performed at a much higher level than that of E687 in spite of the much higher particle flux environment.

A hadron track can be misidentified as a muon if there is a real muon track close by which causes hits in the muon detector. One can greatly reduce such misidentification by requiring that the putative muon be "isolated", that is that no other track be identified as a muon on the basis of the same muon hits. Our routine calculates such an "isolation" variable and we have demonstrated its usefulness by testing it on samples where we have alternative ways of identifying the hadron.

The reduction of misidentification due to pions decaying in flight requires the use of data from other detectors. The UPR was successful in implementing software to do this using the information from two detector systems: the momentum-measuring PWC chambers and the Cerenkov detectors. In one case one uses the difference in the momentum measured by the first and the second analysis magnets. In the other case one uses the Cerenkov system to differentiate pions from muons (in a limited momentum range). Although this is a very challenging problem, these algorithms will be very useful in future detailed data analysis where the reduction of background to a minimum will be crucial.

Another analysis project was directed to the utilization of the timing data from the Cerenkov signals for the purpose of determining if a given track came from the triggering event or not. Software was developed to calibrate the timing of individual counters (300 total) and to calculate the timing period to which each Cerenkov signal as well as each particle trajectory were associated. The use of these routines to reduce background in real signals was studied. In some cases a reduction of 38% in background was achieved with only an 8% reduction in yield.

The primary processing of the FOCUS data (Pass1) which required the large CPU power available only at Fermilab ran continuously for ten months. Control and monitoring of this process was carried out by the members of the collaboration via Internet. Our group did its assigned part in carrying out this task.

The product from Pass1 was a set of 6000 secondary data tapes which contain all the reconstructed events. The pre-selection and partitioning of events into reasonably small data sets was a two-part process. Skim1 was carried out at two of our collaborating institutions with large processing

capacity (University of Colorado and Vanderbilt University). Skim1 produced six large data streams (superstreams) each containing approximately 500 data tapes with events selected on the basis of gentle requirements to assure that no signals were rejected.

Skim2 was carried out at five institutions. Each one worked with a superstream to further partition it into substreams each consisting of less than 50 tapes. Our cluster was responsible for Superstream1. As part of this task a skimming system was developed at Mayaguez. There were two aspects involved. One was the determination of the criteria to be used in the partitioning of events into substreams. The other was the implementation and adaptation of a data handling and analysis system which would allow an efficient skimming process with maximum control and monitoring capabilities.

The large number of data input and output tapes involved led the collaboration to develop a sophisticated skimming system with control and monitoring via a local Intranet and continuous interaction with central databases maintained at Fermilab which contain the information on the processing of each data tape. At Mayaguez we adapted this system to our particular computing environment and added the refinement of parallel distribution of processing tasks to various computing nodes.

Superstream1 consisted mainly of semileptonic and dileptonic events to be subdivided into five substreams. The development of partitioning criteria required a study on real and simulated data of the effects of varying several selection requirements. The input to the skim consisted of 290, 8mm tapes each containing approximately 4Gb of data and requiring 200 minutes of CPU processing time in our Alpha Unix workstations. With our parallel distribution system, the analysis of the data occurred at effective rates two to three times faster than tape reading speed allowing us to read in several tapes simultaneously. In our best day (24 hours), we skimmed thirty input tapes and wrote out twenty output tapes. A total of 191 output tapes were written.

Appendix D

Semileptonic Analysis in FOCUS

$\frac{\Gamma(D^+ \to \rho^0 \mu^+ \nu)}{\Gamma(D^+ \to \overline{K^{*0}} \mu^+ \nu)}$ Analysis in FOCUS

Eduardo E. Luiggi and Angel M. Lopez

October 2003

D.1 Data Selection

D.1.1 Skims

The data for this analysis was taken from the Skim2 semimuonic sub-sample (FSAA). This skim required the events to have at least one muon and a meson in the final state with a minimum L/σ separation of 1.5 and a secondary vertex confidence level greater than 1%. The meson in the event could be either a pion or a kaon.

This sample was subjected to Skim3 which was designed to select events with two mesons and a muon forming a vertex with a confidence level exceeding 1% and L/σ separation greater than 5. The mesons could be either two pions (ρ^0), two Kaons (ϕ) or a Kaon-pion combination (K^{*0}). The pion or pions in the event were required to be pion consistent (piconicity > -7) while tracks with kaonicity greater than -1 were identified as Kaons. The muons were required to have $CL_{imu} > 0.01$ and $p_\mu > 10$ GeV or $CL_{omu} > 0.05$ and $p_\mu > 4$ GeV. The events that passed all the above cuts were divided into three different sub-samples according to their meson combination. Both our $D^+ \to \rho^0 \mu^+ \nu$ sample as our $D^+ \to \overline{K^{*0}} \mu^+ \nu$ sample used for normalization were taken from this skim.

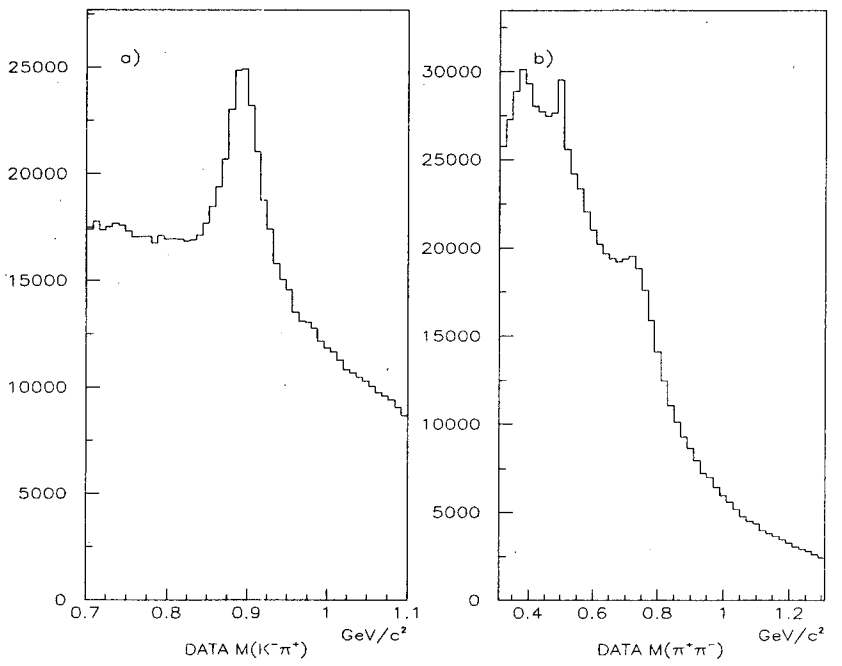

Figure D.1: Invariant mass distributions for all events that passed Skim Three. a) $D^+ \to \overline{K^{*0}}\mu^+\nu$ candidates, b) $D^+ \to \rho^0\mu^+\nu$ candidates.

D.1.2 Analysis Cuts

In the course of this analysis we have identified three major sources of backgrounds:

1. Charm semileptonic decays with two pions in the final state (plus some neutral particle).
2. Combinatoric Background
3. Muon misidentification

The cuts described below were chosen because they maximize our yield while keeping the amount of background present in our signal area under control.

We started the $D^+ \to \rho^0\mu^+\nu$ analysis looking for a secondary vertex with two opposite charge pions and a muon outside the target material by three sigmas. This vertex was required to have $CL_{sec} > 5\%$

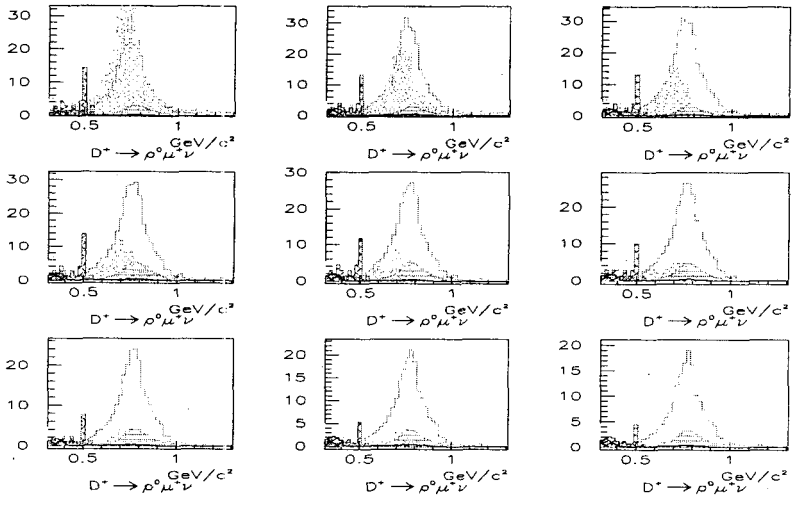

Figure D.2: Pionicity cut effect on the semileptonic contributions. The cut was varied from 0 to 8. The green histogram are $D^+ \to \overline{K^{*0}}\mu^+\nu$ misidentifi ed as $D^+ \to \rho^0\mu^+\nu$.

and Iso2 $< 5\%$. The minimum L/σ used was 15. The primary vertex was found in the usual way, excluding the secondary tracks from the search and looking for the vertex with the highest multiplicity. The requirements for this vertex were: $CL_{prim} > 1\%$ and Iso1 $< 1\%$.

In order to get a cleaner signal, only muons from the Inner Muon System were used in our analysis. The muon candidate was required to have a momentum greater than 10 GeV and $CL_{imu} > 1\%$. Pion identification was done different for each pion in the vertex depending on the sign of the pion with respect to that of the muon. The pion with the same charge as the muon was required to have pionicity > 0, while the pion with opposite charge as the muon was required pionicity > 5. This was done to reduce the background coming from $D^+ \to \overline{K^{*0}}\mu^+\nu$, $\overline{K^{*0}} \to K^-\pi^+$, where the Kaon is misidentified as a pion. Monte Carlo studies have shown, that this cut can keep the "efficiency" for $\overline{K^{*0}}$ events in our signal area well below 0.01%, while keeping the ρ^0 efficiency high. Figure D.2 shows the effectiveness of this cut reducing contamination from $D^+ \to \overline{K^{*0}}\mu^+\nu$.

Backgrounds from $D^{*0} \to D^0\pi^+, D^0 \to \pi^-\mu^+\nu$, were suppressed requiring a minimal invariant mass difference $M(\pi^+\pi^-\mu^+) - M(\pi^-\mu^+) > 0.20$, while other semileptonic decays that will be discuss later, were reduced with a cut in the invariant mass of the three charge tracks, $1.2 < M(\pi^+\pi^-\mu^+) < 1.8$.

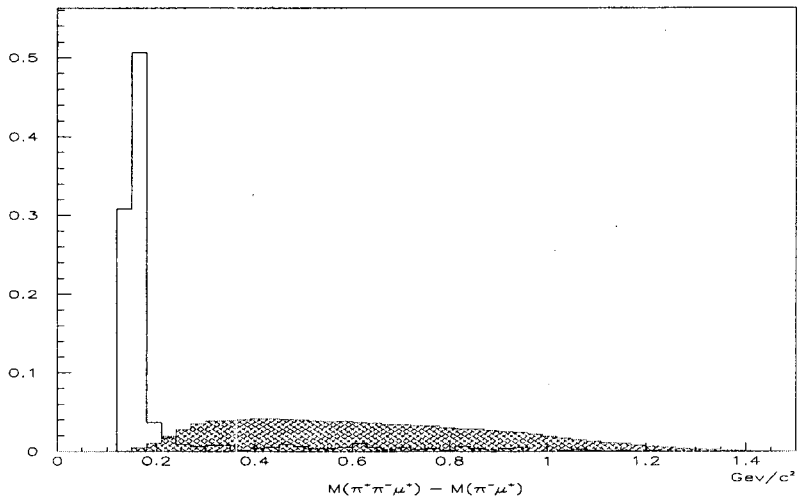

Figure D.3: $M(\pi^+\pi^-\mu^+) - M(\pi^-\mu^+)$ for $D^{*0} \to D^0\pi^+, D^0 \to \pi^-\mu^+\nu$ events (solid histogram) compared to $D^+ \to \rho^0\mu^+\nu$ events (hatched histogram). Both distribution are normalize to unity. The vertical line represents the cut we are applying to our data.

The usefulness of the $M(\pi^+\pi^-\mu^+) - M(\pi^-\mu^+)$ cut is demonstrated in Figure D.3. Events where one of the pion comes from the primary, but it is erroneously assigned to the secondary, can effectively eliminated with the use of this cut.

The non-charm combinatoric background was modeled using events where the two pions had the same charge.The last source of background comes from muon misidentification. To assess the amount of muon misidentification, we took a sub-sample of approximately 10 % of the FOCUS data and performed the same analysis with opposite muon requirements (e.g.,$CL_{imu} < 1\%$) and plot $M(\pi^+\pi^-)$. Then, we weighted this histogram with a momentum dependent misidentification probability function and boosted it by the ratio of the amount of charm decays in the full sample to the amount of charm decays in our sub-sample.

To reduce systematic uncertainties arising from our cut selection, we applied the same cuts to our $D^+ \to \overline{K^{*0}}\mu^+\nu$ normalization sample except for those cuts regarding Kaon identification.

D.2 Fitting Technique

Our $D^+ \to \rho^0\mu^+\nu$ yield was estimated using a binned maximum log likelihood technique. The likelihood was constructed as:

$$\mathcal{L} = \prod_{i=1}^{\#bins} \frac{n_i^{s_i} e^{-n_i}}{s_i!} \tag{D.1}$$

where:

s_i =number of events in bin i of data histogram;

n_i =number of events in bin i of fit histogram.

The fit histogram was composed of the following:

1. $D^+ \to \rho^0\mu^+\nu$ signal, whose shape was given by the Monte Carlo and the yield was a fit parameter.

2. Feed-through from $D^+ \to \overline{K^{*0}}\mu^+\nu$, $(K/\pi Mis - id)$ with shape given by Monte Carlo and the yield depended on the $D^+ \to \overline{K^{*0}}\mu^+\nu$ efficiency corrected yield.

3. $D^+ \to \overline{K^0}\mu^+\nu$, with shape given by Monte Carlo and yield determined as a fit parameter.

4. Various backgrounds from $D_s^+ \to \eta'\mu\nu$ and $D_s^+ \to \eta\mu\nu$, whose yields depended on $D_s^+ \to \phi\mu^+\nu$ efficiency corrected yield and on the PDG values for $\frac{BR(D_s^+ \to \eta'\mu\nu)}{BR(D_s^+ \to \phi\mu\nu)}$ and $\frac{BR(D_s^+ \to \eta\mu\nu)}{BR(D_s^+ \to \phi\mu\nu)}$ respectively.

5. $D_s^+ \to \phi\mu^+\nu$, $\phi \to \rho^0\pi^0$, with shape determined by Monte Carlo and yield depend on $D_s^+ \to \phi\mu^+\nu$ efficiency corrected yield and on the PDG value for BR($\phi \to \rho^0\pi^0$).

6. Combinatoric background, with shape given by same sign pions from the data.

7. Muon Mis-Id, with shape given by data and yield was fixed in the fit.

The number of entries in bin i of the fit histogram was defined as:

$$
\begin{aligned}
n_i =& Y_{\rho\mu\nu} S_{1i} + \frac{Y_{\overline{K^{*0}}\mu^+\nu}}{\epsilon(\overline{K^{*0}}\mu^+\nu)} \epsilon(\overline{K^{*0}}\mu^+\nu \to \rho\mu\nu) S_{2i} + \\
& Y_{D^+\to\overline{K^0}\mu\nu} S_{3i} + \frac{Y_{D_s^+\to\phi\mu^+\nu}}{\epsilon(D_s^+ \to \phi\mu^+\nu) BR(\phi \to KK)} BR(\phi \to \rho^0\pi^0) S_{4i} + \\
& \frac{Y_{D_s^+\to\phi\mu^+\nu}}{\epsilon(D_s^+ \to \phi\mu^+\nu) BR(\phi \to KK)} \Big\{ BR_{\eta'} \cdot \Big[BR(\eta' \to \rho\gamma)\epsilon(\eta' \to \rho\gamma) S_{5i} + \\
& BR(\eta' \to \eta\pi\pi)\epsilon(\eta' \to \eta\pi\pi) S_{6i} \Big] + BR_\eta \cdot \big(BR(\eta \to \pi\pi\pi^0)\epsilon(\eta \to \pi\pi\pi^0) S_{7i} + \\
& BR(\eta \to \pi\pi\gamma)\epsilon(\eta \to \pi\pi\gamma) S_{8i} \big) \Big\} + \mathcal{C} S_{9i} + \mathcal{M} S_{10i}
\end{aligned}
\tag{D.2}
$$

where:

$Y_{\rho\mu\nu}$ is the fitted yield for $D^+ \to \rho^0\mu^+\nu$; $\frac{Y_{\overline{K^{*0}}\mu^+\nu}}{\epsilon(\overline{K^{*0}}\mu^+\nu)}$ is the efficiency corrected yield for $D^+ \to \overline{K^{*0}}\mu^+\nu$; $BR_{\eta'} = \frac{BR(D_s^+\to\eta'\nu)}{BR(D_s^+\to\phi e\nu)}$; $BR_\eta = \frac{BR(D_s^+\to\eta e\nu)}{BR(D_s^+\to\phi e\nu)}$; $Y_{D^+\to\overline{K^0}\mu\nu}$ is the fitted yield for $D^+ \to \overline{K^0}\mu\nu$; $\mathcal{C}$ is the fitted Combinatoric Background; $\mathcal{M}$ is the fixed Muon Mis-Id; S_i are normalized Monte Carlo shapes and BR are Branching Ratios from PDG. The signal was fitted using the range from 0.31MeV/c^2 to 1.31MeV/c^2.

The normalization sample was fitted with a constant width Breit Wigner after subtracting the wrong sign events.

D.3 Results

D.3.1 Fit Results

Table D.1 shows the different sources that constitutes our $D^+ \to \pi^+\pi^-\mu^+\nu$ spectrum and the number of events that each contribute to the signal. We found a total of 273 ± 34 $D^+ \to \rho^0\mu^+\nu$ events.

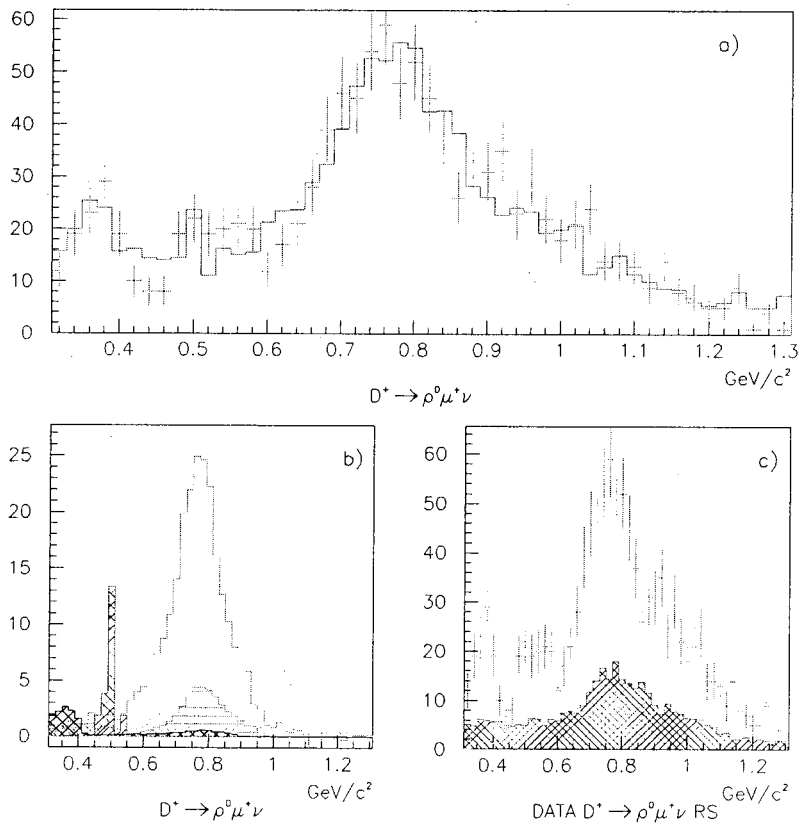

Figure D.4: $D^+ \to \rho^0\mu^+\nu$ Fit Result. Figure a shows the fi t result (solid histogram) over the data (ploted with error bars. Figure b shows the semileptonic contributions while Figure c shows the muon mis-identifi cation and combinatoric backgrounds.

D.3.2 $\frac{\Gamma(D^+\to\rho^0\mu^+\nu)}{\Gamma(D^+\to\overline{K^{*0}}\mu^+\nu)}$ Results

The $\frac{\Gamma(D^+\to\rho^0\mu^+\nu)}{\Gamma(D^+\to\overline{K^{*0}}\mu^+\nu)}$ branching ratio was calculated using the double ratio method discussed in [1].

$$\frac{\Gamma(D^+ \to \rho^0\mu^+\nu)}{\Gamma(D^+ \to \overline{K^{*0}}\mu^+\nu)} = \frac{Y_\rho^{(data)}}{Y_{K^{*0}}^{(data)}} \times \frac{Y_{K^{*0}}^{(MC)}}{Y_\rho^{(MC)}} \times RelBR^{(MC)} \tag{D.3}$$

where $Y_{\rho}^{(data)}$, $Y_{K^{*0}}^{(data)}$, $Y_{K^{*0}}^{(MC)}$ are the fitted yields for $D^+ \to \rho^0\mu^+\nu$(data) and $D^+ \to \overline{K^{*0}}\mu^+\nu$(data and MC), $Y_{\rho}^{(MC)}$ is the number of events in our MC histogram and $RelBR^{(MC)}$ is the $\frac{\Gamma(D^+\to\rho^0\mu^+\nu)}{\Gamma(D^+\to\overline{K^{*0}}\mu^+\nu)}$ relative branching ratio assumed by the MC.

Using the above results we obtain the following $\frac{\Gamma(D^+\to\rho^0\mu^+\nu)}{\Gamma(D^+\to\overline{K^{*0}}\mu^+\nu)}$ relative branching ratio:

$$\frac{\Gamma(D^+ \to \rho^0\mu^+\nu)}{\Gamma(D^+ \to \overline{K^{*0}}\mu^+\nu)} = 0.043 \pm 0.005(stat) \pm 0.005(syst)$$

D.4 Systematic Uncertainties

Systematic uncertainties were estimated following the approach described in [2]. This method uses three basic technique to assess systematic uncertainties.

1. Cut variants
2. Fit variants
3. Split sample

Systematic uncertainties due to our cut selection were studied recalculating our branching ratio using different cut combinations. We studied a total of 192 cut combinations were the values for the secondary

Decay Mode	Yield
$D^+ \to \rho^0\mu^+\nu$	273
$D^+ \to \overline{K^{*0}}\mu^+\nu, K/\pi Mis-id$	63
$D^+ \to \overline{K^0}\mu\nu$	35
$D_s^+ \to \eta'\mu\nu, \eta' \to \rho^0\gamma$	33
$D_s^+ \to \eta'\mu\nu, \eta' \to \eta\pi\pi$	1
$D_s^+ \to \eta\mu\nu, \eta \to \pi\pi\pi^0$	24
$D_s^+ \to \eta\mu\nu, \eta \to \pi\pi\gamma$	8
$D_s^+ \to \phi\mu^+\nu, \phi \to \rho\pi$	11
Muon Mis-Id	347
Combinatoric	311

Table D.1: Semileptonic Contributions to $D^+ \to \pi^+\pi^-\mu^+\nu$ signal

vertex CL, secondary isolation CL, out of material cut and pionicity of the pion with opposite charge to that of the muon were changed. The systematic uncertainty associated with these cut variations is the variance of measured branching ratios. We quote a systematic uncertainty due to the cut selection of: $\sigma_{syst} = 0.003$. Figure D.5 show the branching ratio for the 192 cut combinations.

For the systematic due to our fitting technique we changed the bin size used to plot our data, the mass range used, the values for the branching ratios used to calculate the semileptonic backgrounds contributions and the Corrected yield for the $D^+ \rightarrow \overline{K^{*0}}\mu^+\nu$used to estimate the amount of kstar present in our signal. The systematic uncertainty due to this changes was calculated to be $\sigma_{syst} = 0.002$.

Split sample systematic were studied dividing our sample into two sets depending upon the D^+ momentum, run number and particle-antiparticle. The systematic uncertainty was $\sigma_{syst} = 0.003$. Combining these systematic uncertainties in quadrature we obtained a total systematic uncertainty of $\sigma_{syst} = 0.005$. Table D.2 show the three contributions to our total systematic uncertainty.

Source	Syst
Cut	0.003
Fit	0.002
Split	0.003
Total	0.005

Table D.2: $D^+ \rightarrow \rho^0\mu^+\nu$ Systematic Sources

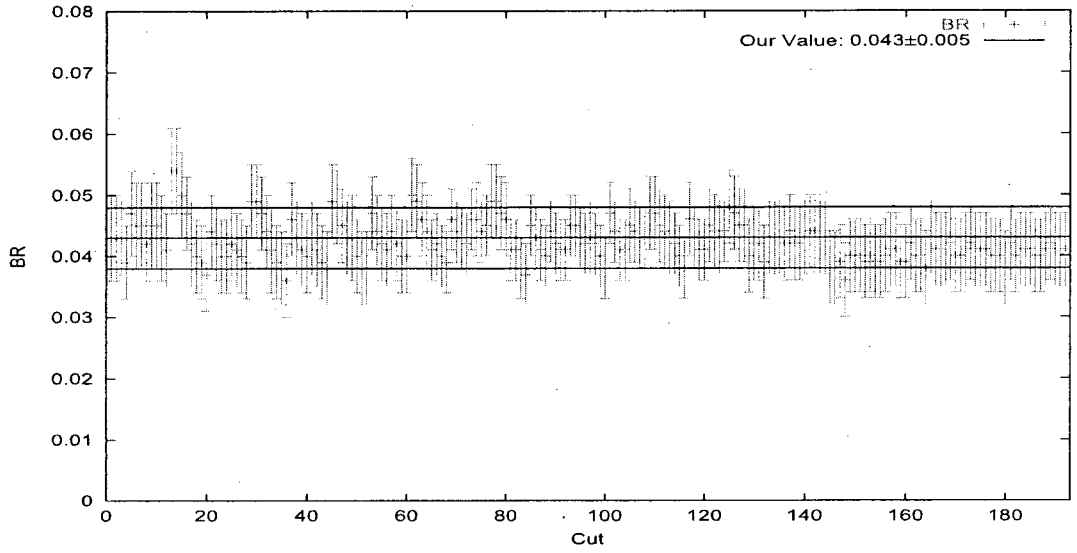

Figure D.5: Cut variants Branching ratios

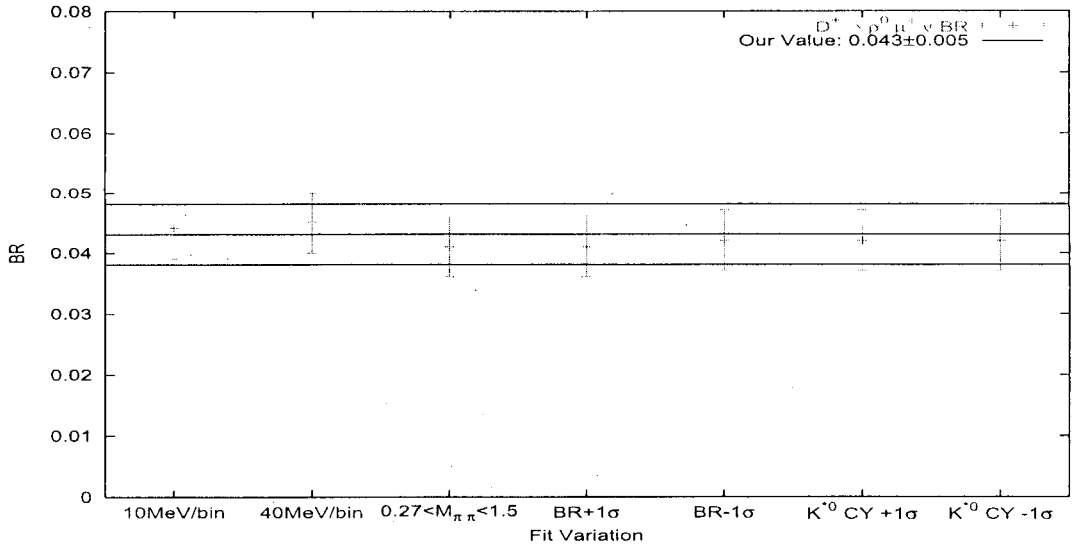

Figure D.6: Fit variants Branching ratios

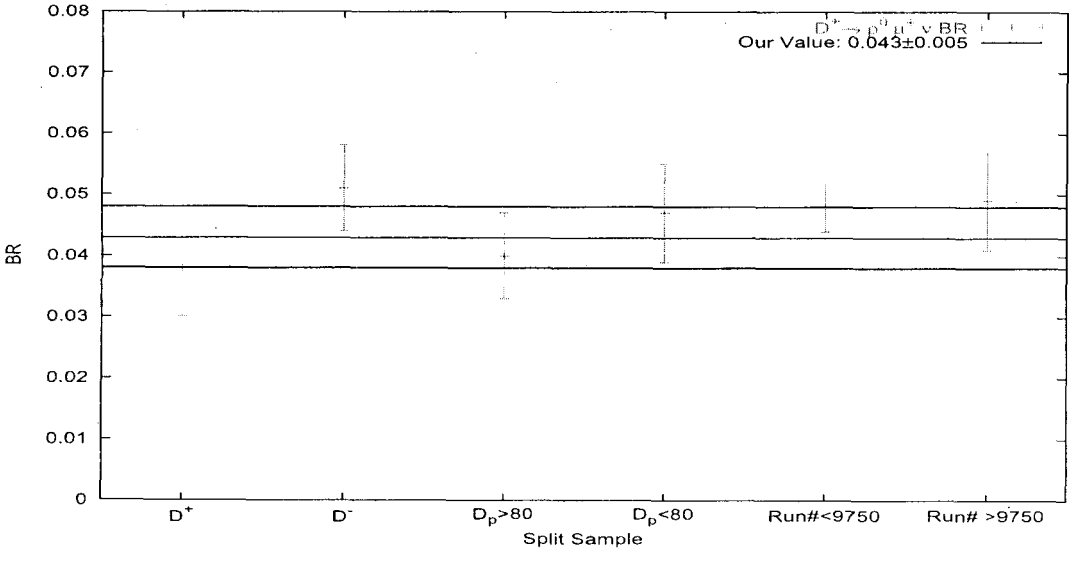

Figure D.7: Split Sample Branching ratios

Bibliography

[1] D. Kim, J. E. Wiss, "Progress on the $\frac{\Gamma(D^+ \to \overline{K^{*0}}\mu^+\nu)}{\Gamma(D^+ \to K^-\pi^+\pi^+)}$ Relative Branching Ratio," E831 Internal Memo, 2002.

[2] R. Gardner, J. E. Wiss, "Estimating Systematics Errors," E831 Internal Memo, 1994.

Appendix E

A Search for the Rare Decay $D^0 \to \mu^+\mu^-$

A Search for the Rare Decay $D^0 \to \mu^+\mu^-$

by
Hugo R. Hernández and Angel M. López
University of Puerto Rico
Mayagüez Campus
June 6, 2003

Abstract

We report on a search for the rare decay $D^0 \to \mu^+\mu^-$ based on data collected by the Fermilab fixed target photoproduction experiment FOCUS (FNAL-E831). This decay is an example of a flavor-changing neutral-current process which, according to the Standard Model, should occur at a very low branching ratio of at most 10^{-13}. The optimum selection criteria for candidate events was determined using a blind analysis method. A dual bootstrap method was used to adjust the sensitivity for bias due to possible fluctuations in the background sample. The ratio of background outside to background inside the signal region was determined using an independent real data sample and a Monte Carlo simulation. The result for the sensitivity of the $D^0 \to \mu^+\mu^-$ decay at 90% Confidence Level upper limit is 2.7×10^{-6} which would imply a reduction to the published value for the branching ratio, which is 4.1×10^{-6}.

1 Introduction

The Standard Model of electroweak interactions is used to understand the decays of heavy quarks which are known to us. An observation of a high rate of charm Flavor-Changing Neutral-Current decays, predicted to occur rarely in the Standard Model, would imply new physics beyond the Standard Model.

Rare decay modes are probes of non-standard particle states or mass scales which cannot be accessed directly. One of the most interesting processes to study is the $D^0 \to \mu^+\mu^-$ decay[1]. The main goal of the work reported in this document was the determination of the FOCUS sensitivity for this decay.

2 FCNC Decay Theory

The fundamental work concerning FCNC decays is the famous paper by Glashow, Iliopoulos and Maiani in which they propose the existence of the charm quark and discuss how it can explain the suppression of FCNC decays [1] through what is now called the GIM mechanism.

With respect to $D^0 \to \mu^+\mu^-$ which is a charm FCNC decay, the GIM mechanism leads to suppression of the tree-level diagrams such as Figure 1.a. In a 1997 paper [2], Pakvasa presented a calculation for this process. He found that the short distance effects are dominated by internal s-quark loop diagrams which are suppressed by the smallness of the s quark mass and by helicity considerations.

[1] all references to this decay also implies the corresponding charge-conjugate state $\overline{D}^0 \to \mu^-\mu^+$

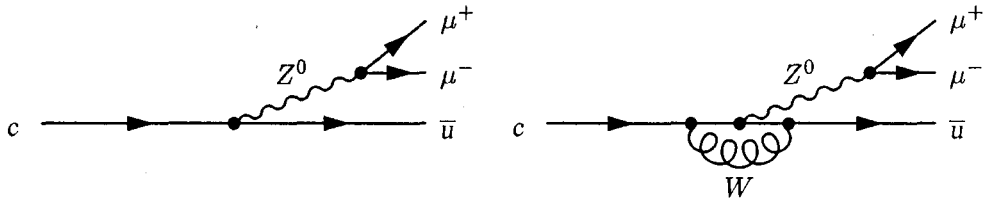

(a) Suppressed Diagram of First Order (b) Penguin Diagram

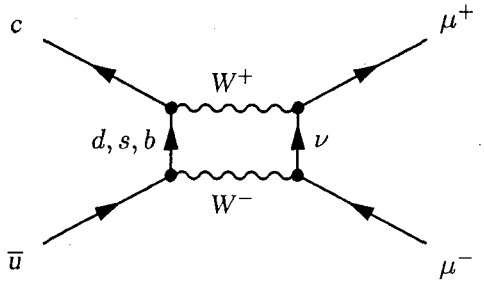

(c) Box Diagram

Figure 1: Feynman diagrams for the decay $D^0 \to \mu^+\mu^-$. (a) represents a suppressed diagram of first order. (b) and (c) are second order diagrams with quark masses d, s, and b within the loops that give a rate proportional to m_s^4, m_s being the mass of the strange quark.

Pakvasa calculated the short distance effects to be of the order of 10^{-19}. However, the long distance effects are larger bringing Pakvasa's calculation of the Standard Model branching ratio to 10^{-15}. The long distance effects are due to intermediate states such as π^0, K^0, $\overline{K}^0$, η, η' or $\pi\pi$ and $K\overline{K}^0$ [2].

Recently, Burdman *et. al.* [3] considered two contributions additional to Pakvasa's consideration for long distance effects, the single-particle "weak-mixing" unitary contribution and, the two-photon unitary contribution, which lead to $D^0 \to \mu^+\mu^-$ transition. They estimate a long distance contribution to the branching ratio for $D^0 \to \mu^+\mu^-$ of at least 3×10^{-13}.

Many experiments have reported limits for the branching ratio of the rare decay $D^0 \to \mu^+\mu^-$. The current 90% Confidence Level upper limit published by PDG [4] is 4.1×10^{-6}. Thus, there is a large window for finding physics beyond the Standard Model in this decay. Burdman *et. al.* estimates the effects of many such extensions. Some are as large as 3.5×10^{-6}.

3 Data Selection

FOCUS utilized a forward large aperture fixed-target multi-particle spectrometer to measure the interactions of high energy photons on a segmented BeO target. There are 6.5 billion photon interaction events on about 6000

8 mm magnetic tapes which constitute the raw data set of the experiment. The primary analysis was divided into three steps: PASS1, Skim1 and Skim2.

After the three FOCUS data selection stages, we proceeded to apply additional selection criteria in a new stage called Skim3 which considered a hadronic trigger requirement. The data in Substream 2 of Superstream 1 was used as the starting point in Skim3.

The main idea of Skim3 was to require the existence of two linked muon candidate trajectories with opposite charge coming from a parent that was identified with a cut in the dimuonic invariant mass around the mass of the D^0 (between 1.7 and 2.1 GeV). Muons (confidence level greater than 1%) could pass the inner muon system or the outer muon system. The primary vertex was found using *DVNUCL*. A confidence level of 1% was required for the secondary dimuon vertex ($CLS > 1\%$). Furthermore, the production vertex was required to be separated from the decay vertex by at least three times the separation error ($\ell/\sigma_\ell > 3$).

Invariant mass distributions with Skim3 selection criteria are shown in Figure 2 for dimuonic as well as normalizing samples. Following the blind analysis methodology (see Section 6.2), only sideband events are presented for the dimuon real data. Figure 2.a shows the dimuonic real data sample, Figure 2.b the $D^0 \to \mu^+\mu^-$ Monte Carlo sample, in Figure 2.c and Figure 2.d we presented the normalizing samples for real as well as Monte Carlo data respectively. The signal region has been masked for the dimuon real data. The real data samples have large background levels with these loose cuts.

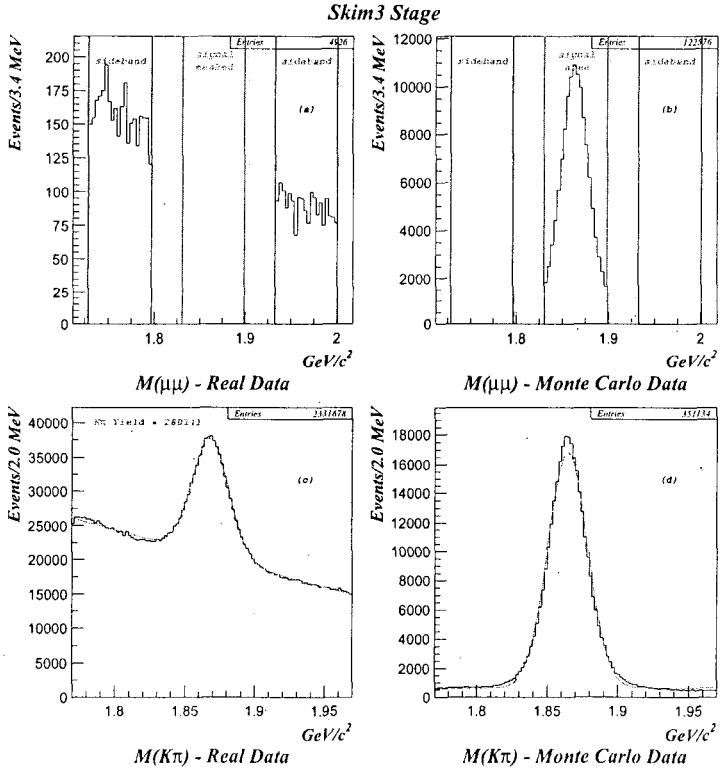

Figure 2: Invariant Mass Distributions for Skim3 Cuts.

At the end of Skim3, we continued to reduce the data by a process which we call Skim4. The selection criteria required for Skim4 were the following:

- $Iso1$ and $Iso2 < 1\%$
- Vertex z position, $-10.0 < z < 2.0$
- $IoT \leq 2.0$
- $N_{prim} \geq 2$
- M_μ momentum > 7 GeV
- CLP and $CLS > 1\%$
- $\ell/\sigma_\ell > 5$
- ($IMUCL > 1\%$ and $MISSPL < 3$ and $K/\mu < 8$ and $TRKFIT\_CL > 1\%$) or OMUCL $> 1\%$

where *Iso1* and *Iso2* are the primary and secondary vertex isolation cut respectively; IoT is the difference between the z vertex position and the z target edge divided by the uncertainty; N_{prim} is the number of trajectories used to form the primary vertex; *CLP* the primary vertex confidence level; *IMUCL* is the inner muon confidence level; *MISSPL* is the number of missed muon planes; K/μ is the kaonicity for muons; *TRKFIT_CL* is a cut which reduces the muon MisID background demanding a consistent SSD-PWC trajectory; and, *OMUCL* is the outer muon confidence level. For this stage was also required that the two muon trajectories must have left a signal in the five PWC chambers.

Figure 3 shows the Skim4 distributions which correspond to the the samples used for our detailed analysis.

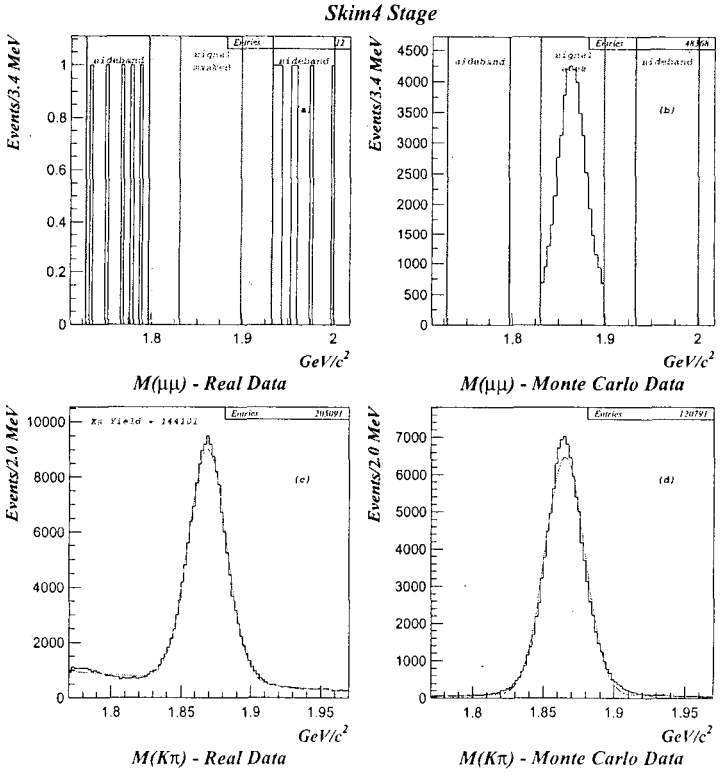

Figure 3: Invariant Mass Distributions for Skim4 Cuts.

4 Normalizing Mode

We will use $D^0 \to K^-\pi^+$ as the normalizing mode and calculate:

$$BR(D^0 \to \mu^+\mu^-) = \frac{N_{obs}(D^0 \to \mu^+\mu^-)}{N_{obs}(D^0 \to K^-\pi^+)} \frac{\epsilon_{K\pi}}{\epsilon_{\mu\mu}} BR(D^0 \to K^-\pi^+) \quad (1)$$

where the ratio $\epsilon_{K\pi}/\epsilon_{\mu\mu}$ corresponds to the *relative efficiency* to be calculated making parallel Monte Carlo simulations for the two processes, $D^0 \to \mu^+\mu^-$ and $D^0 \to K^-\pi^+$. BR($D^0 \to K^-\pi^+$) has been previously measured by other experiments as $3.88 \pm 0.09 \times 10^{-2}$ [4].

The data events for the normalizing mode were selected using the same selection criteria (except for particle identification) used to select the dimuonic data events. The normalizing mode data was obtained from Substream 5 of the Superstream 1. This Substream contained hadronic decays selected with the same basic conditions as the other Superstream 1 events with the specific purpose of serving as a normalization sample.

5 Monte Carlo Simulation

FOCUS used the Pythia 6.127 [5] generator as a Monte Carlo simulator to model charm production by photon interactions with the target material. Pythia generated a $c\bar{c}$ pair where it was possible to specify the type of charm (D^0, D^+, Σ_c^+, etc.) generated and a specific decay path. Typically this was done for one of the charm quarks while the other was left free to hadronize and decay according to the known cross sections and branching ratios.

$D^0 \to \mu^+\mu^-$ Events. To calculate dimuonic efficiencies it was necessary to generate Monte Carlo data which were required to pass through the same selection criteria that were applied to real data, in other words, the requirements set by Pass1, Skim1, Skim2, Skim3 and Skim4. 3,000,000 events were generated for the process $\gamma + p \to (D^0 \to \mu^+\mu^-) + \bar{c}$ represented in Figure 4.

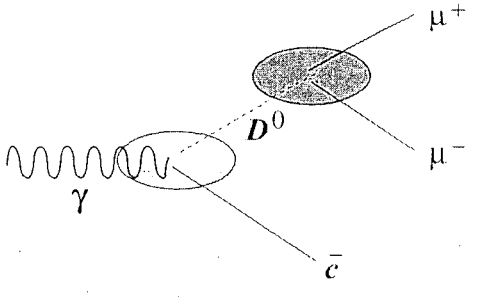

Figure 4: Monte Carlo generated process schematization for the decay $D^0 \to \mu^+\mu^-$.

The number of events provided us with enough sampling statistics to make accurate determinations of the detection efficiencies. Table 1 schematize how the dimuonic Monte Carlo events were generated as suggested by FOCUS (flag values not listed here implies that their values are the default FOCUS settings for Monte Carlo simulations).

$D^0 \to K^-\pi^+$ Events. 3,000,000 $D^0 \to K^-\pi^+$ events were generated. The same selection criteria were applied as with the normalizing data. These events were generated in the same way as dimuonic events.

Table 1: Flags corresponding to the Monte Carlo $D^0 \to \mu^+\mu^-$ events.

MIXEMUP	-1	DOMU	T	PURGE1	T
PRINTLEVEL	3	DOOMU	T	PURGE2	T
TRIGLEVEL	4	DOHC	T	PURGE3	T
OESIMLEVEL	1	DOTRIG	T	PURGE4	T
HCSIMLEVEL	1	IMCS	39	PURGE5	T
EHITYPE	1	PILEMU	0.15	MCBEAMFILE	3
BREM	1	PILE	-1.0	NEWPROD	T

The decay channel $D^0 \to K^-\pi^+$ is very important in this work because this is the normalizing mode used in the BR($D^0 \to \mu^+\mu^-$) measurement. In addition to that, the same decay channel is present as possible background in our dimuonic sample. The processes $D^0 \to \pi^+\pi^-$ and $D^0 \to K^+K^-$ were also considered in the background study. For the first process, 1.5 million events were generated and 4.3 million events for the second.

$c\bar{c}$ Events. A $c\bar{c}$ Monte Carlo generated data that was used with the idea of understanding the existing background present in the dimuonic sample. A $25X$ sample (*FSSE CCBAR* files skimmed as rare decay samples), generated at Vanderbilt University was used for this study.

6 Analysis Methodology

6.1 Optimization of the Selection Criteria

As explained in Section 3, data analysis started with the application of fixed (constant) cuts which correspond to the skimming process including Skim4. Due to correlations, further optimization of the selection criteria required a procedure which considered a large number of cut sets. These consisted of all possible combinations of the preselected cut values for the variables presented in Table 2. The ranges of the variable cuts were chosen on the basis of the experience with previous FOCUS analysis.

K/μ is defined as the kaon consistency for muons, $\Delta W(K\pi)$ is the kaonicity and π_{con} is the pion consistency. A total of *13,122* different cut sets were considered in the analysis (increased in a factor of *9* when considered the Meson ID).

The selection criteria for the normalizing mode was considered in the same way as for the dimuonic sample: Vertexing ID and Meson ID. Due to the dependence on how we reconstructed the vertexing in both samples we used for both cut values mentioned on Table 2 for the Vertexing ID. Meson ID's are independent cuts of Muon ID's and then, we can choose a specific cut value for the Kaon ID as well as for the Pion ID in the normalizing sample. Figure 5 shows the corrected yield compared to the Pion/Kaon ID for all the cut combinations based on the Vertexing ID and the Meson ID cuts. Comparing the three different cut values for each one of the Meson ID's we can conclude that any of these three cuts is correct because the standard deviation is almost the same for anyone of them.

Table 2: Cut values for each variable considered in the optimization process.

Variable Name	Cut Values
→ Vertexing ID	
ℓ/σ_ℓ	$> 5, 7, 9$
CLS	$> 1\%, 5\%, 10\%$
Iso1	$< 10^{-4}, 10^{-3}, 10^{-2}$
Iso2	$< 10^{-4}, 10^{-3}, 10^{-2}$
IoT	$\leq 0, 1, 2$
→ Muon ID	
K/μ	$< 5, 8$
MISSPL	$< 1, 2, 3$
IMUCL	$> 1\%, 3\%, 5\%$
OMUCL	$> 1\%, 3\%, 5\%$
→ Meson ID	
$\Delta W(K\pi)$	$> 1, 3, 5$
$\pi_{\rm con}$	$< 1, 4, 7$

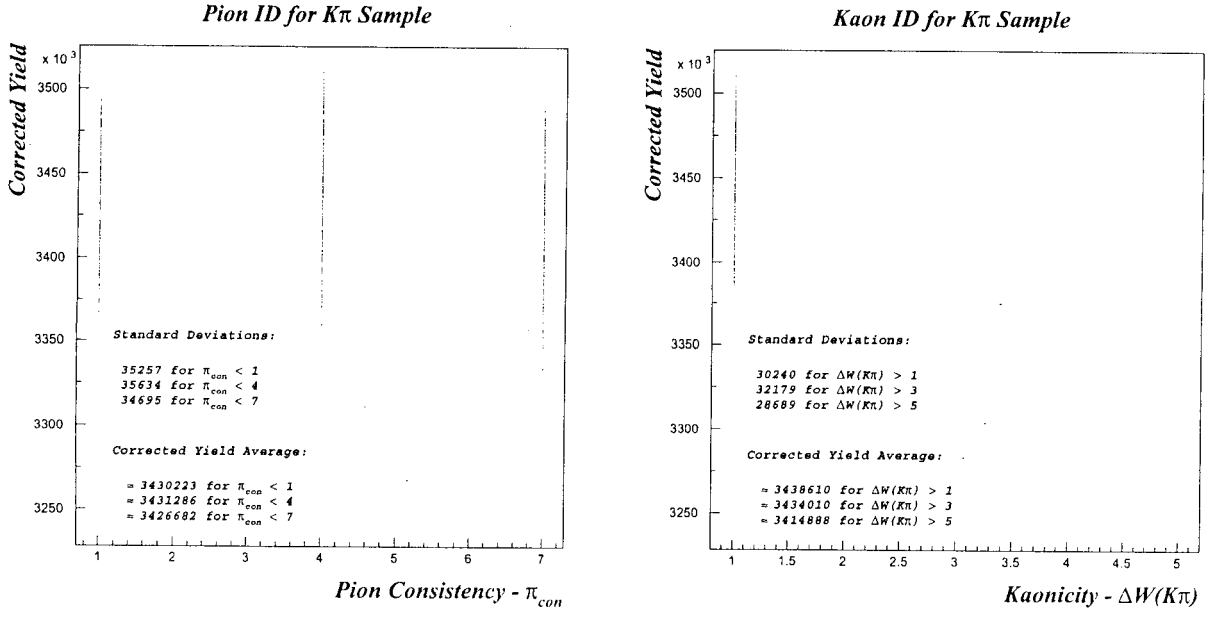

Figure 5: Meson ID for the Normalizing Sample. The standard deviation for any of the cut values used in Kaon ID and Pion ID is almost the same.

6.2 Blind Analysis

Our blind analysis excludes all the events within a defined symmetric area around the value of the D^0 mass in the process of cut selection. This area is called the signal area. In other words, cut optimization is based on reducing

background and not on maximizing the signal under study. The point of this is to avoid having the possible apparent absence or presence of a signal bias the analysis procedure.

6.3 Rolke and López Limits

The statistical method proposed by Rolke and López [6] was used to calculate the confidence intervals and the sensitivities. They suggest a technique to place confidence limits on small signals when background noise is present. This technique is based on a combination of a two dimensional confidence region and a large sample approximation to the likelihood-ratio test statistic. Automatically it quotes upper limits for small signals and also two-sided confidence intervals for larger samples.

The technique of Feldman and Cousins [7] does not consider the amount of uncertainty in the background. The new Rolke and López technique deals with the background uncertainty as a statistical error. The technique performs very well. It has good power and has correct coverage. This method can be used for two situations: when sidebands data give an estimated background rate and when it comes from Monte Carlo. It can also be used if there is a second background source in the signal region.

To understand the results of this technique we will need the following notation: x will represent the observed events in our signal region, y will be the events in the background region and τ will be the ratio of the sidebands background to the signal background. The expected background rate is $b = y/\tau$ and the *Sensitivity Number*, N_B, is defined as the average 90% upper limit for an ensemble of experiments having an average of y events in the sidebands and no true signal.

Table 3 gives the sensitivity numbers for different values of τ and y. Such sensitivities are used in cut optimization. The confidence limits will depend on x as well as on τ and y. Table 4 gives some examples of Rolke and López limits for $\tau = 2$. During the various stages of this analysis, computer routines provided by Rolke and López were used to calculate exact sensitivity numbers and confidence limits.

6.4 Determination of Experimental Sensitivity and Confidence Limits

We define the experimental sensitivity as the average upper limit for the branching ratio that would be obtained by an ensemble of experiments with the expected background and no true signal. Therefore, the experimental sensitivity (S) is calculated in the same way as the branching ratio except that the sensitivity number is used for the number of observed signal events.

$$S(D^0 \to \mu^+\mu^-) = \frac{N_B(D^0 \to \mu^+\mu^-)}{N_{obs}(D^0 \to K^-\pi^+)} \frac{\epsilon_{K\pi}}{\epsilon_{\mu\mu}} BR(D^0 \to K^-\pi^+) \quad (2)$$

where, N_B is the sensitivity number (Section 6.3) which is determined using the Rolke and López routines from the number of events observed in the sidebands, y, and the background ratio, τ. For each particular set of cuts, τ is determined as explained in Section 7.3

In simple terms, the sensitivity is mainly dependent on the ratio of $N_B/\epsilon_{\mu\mu}$. We wish to minimize this ratio which means having low background with high efficiency.

For our final result we will use the dual bootstrap method (Section 6.6) in which many different data sets are analyzed. Leaving aside that complication for now, for each data set the analysis proceeds as follows. The

Table 3: Sensitivity numbers as per Rolke and López. The number of background events in the sidebands is y. The estimated background rate is $b = y/\tau$.

	90% *C.L.*	
y	$\tau = 1$	$\tau = 2$
0	2.21	2.21
1	3.31	2.82
2	3.97	3.17
3	4.62	3.49
4	5.29	4.03
5	5.90	4.23
6	6.37	4.60
7	6.86	4.79
8	7.23	5.14
9	7.64	5.32
10	8.01	5.62
11	8.40	5.78
12	8.71	6.08
13	9.09	6.19
14	9.39	6.45
15	9.71	6.59

Table 4: An example of Rolke and López 90% Confidence Limits. y is the number of events observed in the background region and x is the number of events observed in the signal region. A value of $\tau = 2$ has been assumed.

	y				
x	0	1	2	3	4
0	0,2.21	0,2.27	0,1.58	0,1.28	0,0.9
1	0,3.65	0,3.22	0,3.44	0,3.06	0,2.87
2	0.42,5.3	0,4.87	0,4.43	0,4	0,4.41
3	0.97,6.81	0.08,6.37	0,5.93	0,5.49	0,5.05
4	1.54,8.25	0.74,7.8	0.03,7.36	0,6.91	0,6.47
5	2.16,9.63	1.42,9.18	0.74,8.73	0.07,8.28	0,7.83
6	2.82,10.98	2.12,10.53	1.45,10.08	0.8,9.62	0.17,9.17
7	3.5,12.3	2.83,11.84	2.18,11.39	1.54,10.94	0.91,10.48
8	4.2,13.59	3.55,13.14	2.91,12.68	2.29,12.23	1.67,11.77
9	4.92,14.87	4.29,14.42	3.66,13.96	3.04,13.5	2.43,13.05
10	5.66,16.14	5.03,15.68	4.42,15.22	3.81,14.77	3.21,14.31

optimum cut set is determined as that having the minimum experimental sensitivity. The confidence limits are found by determining how many events are in the signal region for the optimum cut set.

6.5 Sidebands Background and Signal Area

In this analysis, the signal area as well as the sidebands were defined from the invariant mass distribution of Monte Carlo generated data (Figure 6a). The ability of the FOCUS Monte Carlo to predict signal width has been verified with other copious charm signals.

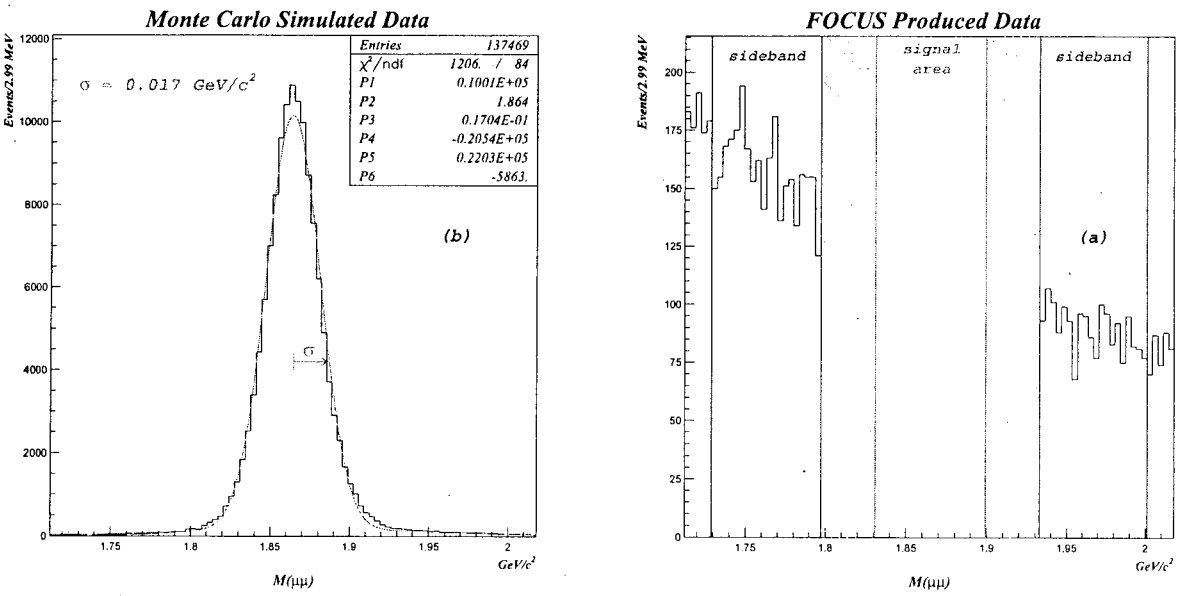

Figure 6: $D^0 \to \mu^+\mu^-$ Invariant Mass distributions. (a) distribution for generated Monte Carlo data with a gaussian fit. The gaussian width is equal to 0.017 GeV. (b) Representation of the sidebands and the signal area for the FOCUS produced data showing the signal and sideband areas. Skim3 cuts have been applied and the signal area has been masked.

The width of the invariant mass distribution for $D^0 \to \mu^+\mu^-$ events is approximately equal to $\sigma = 0.017$ GeV. The signal area was taken as $\pm 2\sigma$ around a D^0 mass of 1.865 GeV [4]. Each one of the sidebands had a width equal to the signal area width but the sidebands were not located immediately next to the signal area. Between each sideband and the signal area, a buffer area was left with a width also equal to 2σ. In this way the left sideband was defined as $1.729 < M_{\mu\mu} < 1.797$ and right sideband $1.933 < M_{\mu\mu} < 2.001$ as shown in Figure 6b.

6.6 Dual Bootstrap

The dual bootstrap method [8] was used for correcting the bias present even in a blind analysis from the fact that there exist statistical fluctuations in the background sample.

Rolke and López have developed this method for rare decays. The procedure for the dual bootstrap in our dimuonic analysis consists of the following steps:

1. create a base sample of dimuonic candidate events by using the loosest cuts in the set of variable cuts (Skim4 sample),
2. create a bootstrap sample from the base sample, then calculate the sensitivity of the bootstrap sample for all the cuts in the variable set of cuts, and find the cut combination which produces the best sensitivity,
3. create a second bootstrap sample from the base sample, calculate the sensitivity for this second bootstrap sample using the best cut combination determined for the first bootstrap sample,
4. repeat steps (2) and (3) 5,000 times and produce a distribution of sensitivities. The median of the distribution of dual bootstrap sensitivities is the measure of the corrected sensitivity,
5. Open the box, i.e., calculate the limits for each of the 5,000 dual bootstrap samples. The median of the limit distributions both upper and lower will constitute the quoted results.

Up to now we have performed the steps through step 4.

7 Background Study

7.1 Introduction

The most important aspect of the analysis is the choice of a set of selection criteria which optimize the probability of observing the signal if it is present. Generally this choice will not be one which eliminates all background because such cuts usually reduce the efficiency of detection of the signal to unacceptably small values. It is therefore important to be able to predict the background level accurately in order to measure the significance of the candidate events. Due to the uncertainties in simulating the background, our analysis methodology relies mainly on the real data (in the sidebands) to predict the background in the signal. However, this methodology requires a determination of the ratio of sideband to signal background, τ. This, in turn, requires a determination of the shape of the background. As is explained in this section, this shape is also obtained from real data.

Fortunately, since they are not strongly-interacting, muons are not produced copiously and it is even rarer that a pair of muons is produced in either a production or decay vertex. In addition, events where the pair of muons come from a non-D^0 two-body decay are largely eliminated by the invariant mass cut while those where the muon pair is formed at the production vertex (i.e. those from the Bethe-Heitler process) are eliminated by the ℓ/σ_ℓ cut. In fact, the main source of background in our final sample are events where one or two mesons have been misidentified as muons. Therefore the understanding of the background started with a study of this misidentification using real data. These results were used to validate the capability of the Monte Carlo to simulate this effect. The Monte Carlo was then used to study some known decay processes which could contribute to the background if the decay products were misidentified as muons. Finally, the background ratio was determined from an independent real data sample of events with no muons in the final state by assuming that the background consisted of such events except that both decay products had been misidentified.

7.2 MisID Study

The goal of this study was to determine the misidentification probability as a function of momentum. Samples of real and simulated $K_s^0 \to \pi^+\pi^-$ decays were used for this purpose.

The real data was obtained from 140 raw data tapes. K_s^0 decays were identified with the following requirements: vertex conditions for a pair of opposite charged particles, the two pion trajectories must have left a signal in the five PWC chambers, and the dipionic mass in a range around the K_s^0 mass ($0.477 < M_{\pi\pi} < 0.517$). Furthermore, decay candidates had to have linked trajectories between the silicon detectors and the PWCs. Events which pass these requirements are called Type-9 K_s^0. By determining how many of these trajectories were identified as muons one could determine the misidentification probability as a function of momentum.

A sample of simulated Type-9 $K_s^0 \to \pi^+\pi^-$ decays was generated with Monte Carlo by artificially lowering the K_s^0 lifetime thus forcing the K_s^0 to decay near the target and obtaining a large sample of pions coming from the target. This sample was analyzed in the same way as the real Type-9 K_s^0 data obtaining consistent results between the two samples.

The measurement of the percentage of pions that were misidentified as muons is shown in Figure 7, for which the following muon identification cuts were applied: $IMUCL > 1\%$ and $MISSPL < 2$.

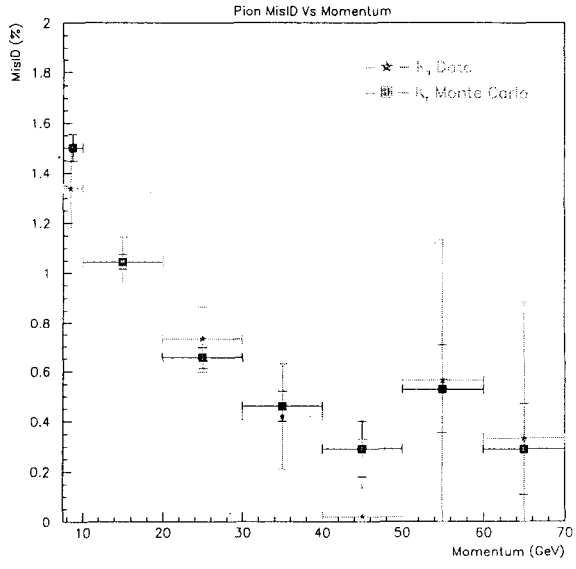

Figure 7: MisID as a function of momentum.

We can see that for low momentum the probability of pion misidentification is greater than for high momentum for real data as well as for Monte Carlo simulated data. This is due to the fact that several effects that contribute to pion MisID, such as pion decays and multiple Coulomb scattering, become larger at low momentum. The results from data and Monte Carlo are consistent within errors.

7.3 Background Ratio Study

In order to have a rough idea of the nature of the background, Monte Carlo was used to generate two-body mesonic D^0 decays which were expected to contribute significantly to the background. The first decay simulated was $D^0 \to \pi^+\pi^-$. Figure 8 (left) shows the comparison of the dimuonic invariant mass distributions for $D^0 \to \mu^+\mu^-$ and $D^0 \to \pi^+\pi^-$. The $D^0 \to \pi^+\pi^-$ peak is slightly shifted from the D^0 mass due to the difference between the pion and muon mass. Since that difference is small, the shift in the peak is small and the invariant mass cut will not help us to eliminate this background. Fortunately, the $D^0 \to \pi^+\pi^-$ decay is Cabibbo-Suppressed and the FOCUS muon system is very good at rejecting pions (low misidentification probabilities).

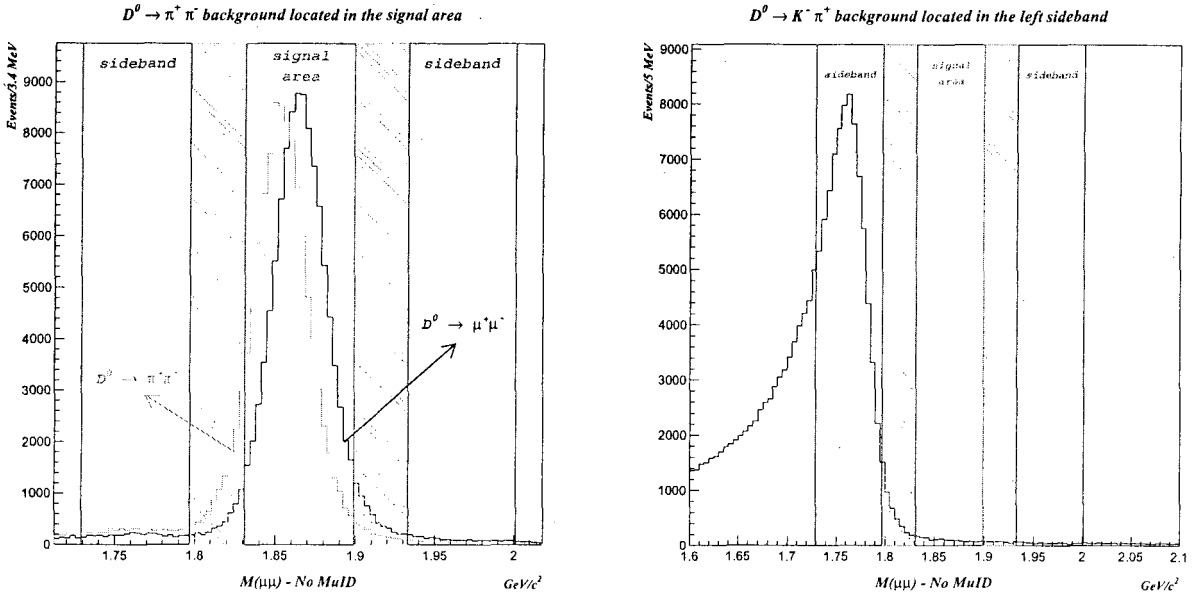

Figure 8: Left: Dimuonic Invariant Mass comparison of Monte Carlo data from $D^0 \to \pi^+\pi^-$ and $D^0 \to \mu^+\mu^-$. Right: Dimuonic invariant mass of $D^0 \to K^-\pi^+$ generated by Monte Carlo.

The other background decay generated was $D^0 \to K^-\pi^+$. Figure 8 (right) shows the dimuonic invariant mass distribution for $D^0 \to K^-\pi^+$ events. Due to the large mass difference between the kaon and the muon, the peak is much more shifted but it does fall within the left sideband. $D^0 \to K^-\pi^+$ is a Cabibbo-Favored decay. Fortunately, it lies outside our signal area and can be almost entirely eliminated by the invariant mass cut. This distribution also shows an additional continuous background inside the signal region. This background is from the other charm particle in the event. It is made up of semimuonic events where the neutrino is not observed or from partially-reconstructed hadronic decays. It is very difficult to simulate all such background components and to know their relative abundance. This is why we do not rely on simulation to obtain the background sideband to signal ratio.

As an alternative to simulation data, a sample of real data from Superstream 2, *SS2*, (also called Global Vertex) was used to determine the background ratio. This superstream was selected with a minimum of requirements and contains all backgrounds to our signal. In particular, no particle identification was used in making SS2. Our procedure consisted in submitting this sample to the same skimming process as the dimuon data except that no muon requirement was used. It was only necessary to work with ~10% of the total SS2 data in order to obtain sufficient statistical power for our purposes (we required *runnum* greater than 9000).

As an example of the dimuonic invariant mass distributions obtained with this procedure, Figure 9 shows the results when one applies tight cuts to the SS2 sample:

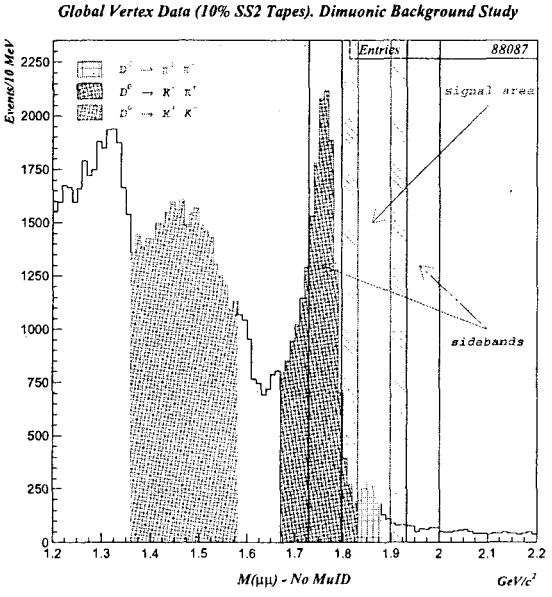

Figure 9: Distribution from SS2 data with tight cuts but no muon identification. These events constitute the main source of background when the decay products are misidentified as muons. There are evident peaks from the processes $D^0 \to K^-\pi^+$, $D^0 \to \pi^+\pi^-$ and $D^0 \to K^+K^-$ along with other background.

The $D^0 \to K^-\pi^+$ is the dominant feature in the distribution but a $D^0 \to \pi^+\pi^-$ peak is also evident as well as other background. The $D^0 \to \pi^+\pi^-$ peak is much smaller than the $D^0 \to K^-\pi^+$ peak because it is Cabibbo-Suppressed. The peak from $D^0 \to K^+K^-$ lies completely outside any region of interest. As the cuts are varied, the ratio of the background in the sidebands to that in the signal (τ) varies but the number of events in the histograms is sufficient to allow a precise determination of this ratio which is calculated using weighted histograms as explained below.

In order to take into consideration the probability of the decay products being misidentified as muons, the background ratio was determined from weighted histograms. Each entry in the dimuonic invariant mass histograms of the SS2 data (such as Figure 9) was weighted with the product of the momentum-dependent MisID probabilities for each of the two decay products. Events with two muons were eliminated from the sample but events with one muon were allowed in order to include semimuonic background. The weight was calculated as follows:

$$w = f_1 * f_2 \tag{3}$$

where $f = 1.0$ for muons, and $f = MisID$ for non-muons. Then, we have that

- $w = MisID1 * MisID2$ if neither decay product is identified as a muon.
- $w = MisID$ if one of the two decay products is identified as a muon.

Figure 10 shows typical weighted invariant mass distributions for Global Vertex data as well as CCBar Monte Carlo generated data. The background ratio τ was calculated by integrating these histogram numerically in the

sidebands as well as in the signal region. A value for the background ratio (τ) was obtained for each of the sets of cuts considered. A comparison between $c\bar{c}$ Monte Carlo generated data and Global Vertex real data is shown in this figure. Both samples were treated with the same selection criteria and we can see that they give highly consistent results for τ.

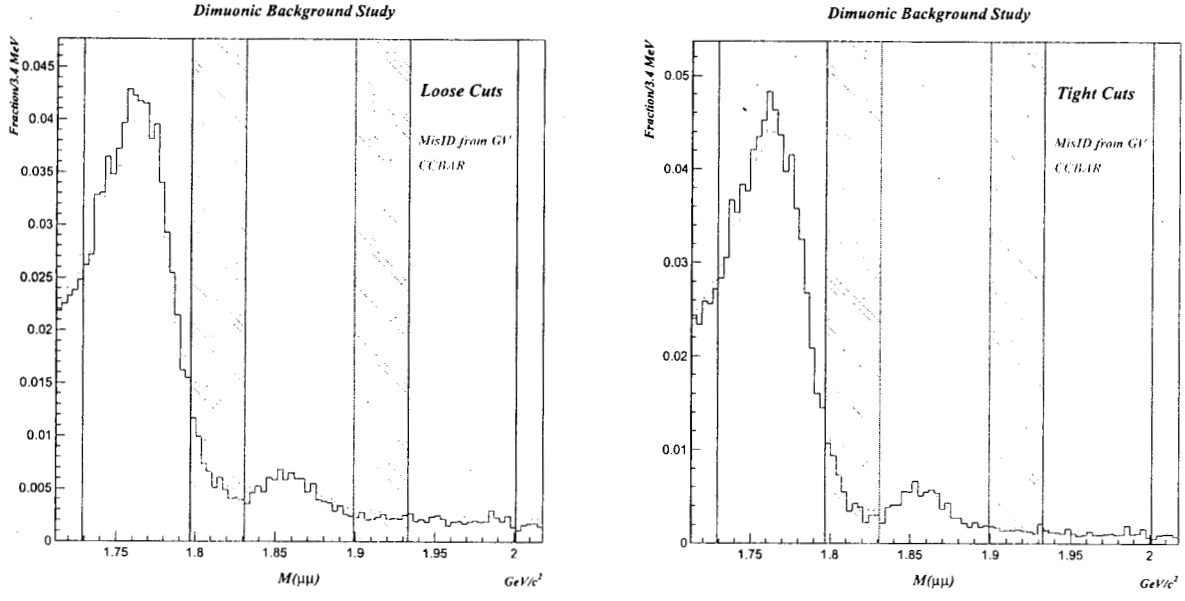

Figure 10: Comparison for CCBar Monte Carlo generated data and Global Vertex real data invariant mass distributions for loose cuts (left) and typical cuts (right). The histograms heve been normalized and weighted by Muon MisID probability as explained in the text.

8 Dual Bootstrap Sensitivity Results

The median of the distribution of dual bootstrap sensitivities (bias-reduced) is 2.7×10^{-6} (Figure 11). This result is encouraging since it is much lower than the existing 90% confidence limit for the branching ratio of 4.1×10^{-6}. This means that our measurement will be more sensitive than previous measurements.

8.1 Typical Results

An example of the results from a typical bootstrap sample are shown in Table 5 and Table 6:

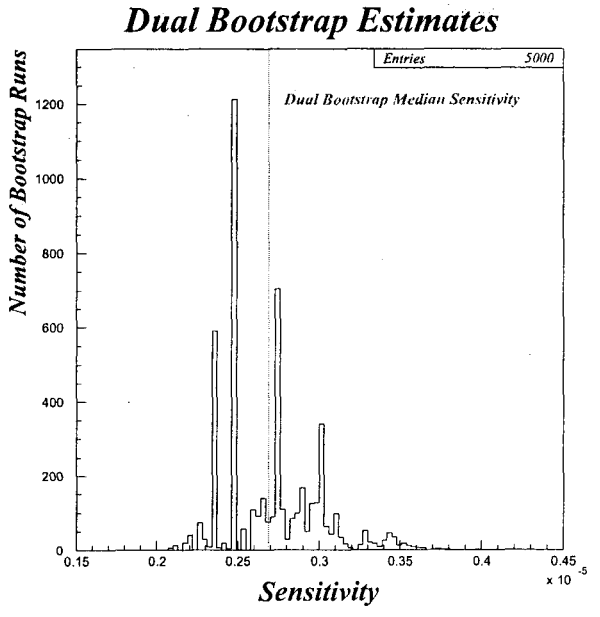

Figure 11: Sensitivity histogram for 5,000 dual bootstrap samples. The median is 2.7×10^{-6}.

Table 5: Best Cut Combination.

$\to$ **Iso1 $<$ 0.1% and Iso2 $<$ 1%**	$\to$ **CLS $>$ 1%**
$\to$ $\ell/\sigma_\ell > 7.0$	$\to$ **IoT $\leq$ 1**
$\to$ **IMUCL $>$ 1%**	$\to$ **OMUCL $>$ 1%**
$\to$ **K/μ $<$ 5.0**	$\to$ **MISSPL $<$ 1**
$\to$ **ΔW(πK) $\geq$ 1.0**	$\to$ $\pi_{\mathrm{con}} \geq -1.0$

Table 6: Results using "typical" cuts.

Background Ratio (τ) :	**4.6**
Predicted Background in Signal :	**0.0**
Sensitivity Number (N_B) :	**2.21**
$D^0 \to \mu^+\mu^-$ efficiency (%):	**1.0**
$D^0 \to K^-\pi^+$ efficiency (%):	**2.8**
$N_{obs}(D^0 \to K^-\pi^+)$:	**107,162**
Sensitivity ($\times 10^{-6}$) :	**2.3**

9 Systematic Errors

The 90% confidence interval upper limit is corrected for systematic errors by the method of Cousins and Highland [9]. Using this method, the increase in the upper limit is given by:

$$\Delta U_n = \frac{1}{2} RL^2 \, \sigma_r^2 \, \frac{RL + b - x}{RL + b} \tag{4}$$

where b is the expected background rate; a signal x; the Rolke and López limit on the signal RL; and a total relative systematic error, σ_r.

For the median of dual bootstrap sensitivities, the corrected limit is:

$$\Delta U_n = \frac{1}{2} RL^2 \, \sigma_r^2 \tag{5}$$

The total relative systematic error is calculated as

$$\sigma_r^2 = \sigma_{\mu-id}^2 + \sigma_{K-id}^2 + \sigma_{HC\ sim}^2 + \sigma_{norm-BR}^2 \tag{6}$$

where $\sigma_{\mu-id}^2$ is the uncertainty in the muon ID efficiency; σ_{K-id}^2 is the uncertainty Kaon ID efficiency; $\sigma_{HC\ sim}^2$ is the triggering uncertainty; and, $\sigma_{norm-BR}^2$ is the uncertainty in the normalizing mode.

10 The Hidden Region

We are ready to open the box for look at $\mu^+\mu^-$ events in the signal region at the data!!!

References

[1] S. Glashow, J. Iliopoulos, and L. Maiani, "*Weak Interactions with Lepton-Hadron Symmetry*," *Physical Review D*, vol. 2, p. 1285, 1970.

[2] S. Pakvasa, "*Symposium on Flavor Changing Neutral Currents: Present and Future Studies*," *FCNC 97*, p. 9, 1997.

[3] G. Burdman, E. Golowich, J. Hewett, and S. Pakvasa, "*Rare Charm Decays in the Standard Model and Beyond*," *Physical Review D*, vol. 66, p. 014009, 2002.

[4] K. Hagiwara *et al.*, "*Review of Particle Physics*," *Physical Review D*, vol. 66, p. 010001, 2002. URL http://pdg.lbl.gov.

[5] T. Sjöstrand, P. Edén, C. Friberg, L. Lönnblad, G. Miu, S. Mrenna, and E. Norrbin, "*High-Energy-Physics Event Generation with PYTHIA 6.1*," *arXiv: hep/ph*, vol. 0010017, 2000.

[6] W. Rolke and A. López, "*Confidence Intervals and Upper Bounds for Small Signals in the Presence of Background Noise*," *Nucl. Inst. and Meth. in Physics Research A*, vol. 458, p. 745, 2001.

[7] G. Feldman and R. Cousins, "*Unified Approach to the Classical Statistical Analysis of Small Signals*," *Physical Review D*, vol. 57, p. 3873, 1998.

[8] W. Rolke and A. López, "*Correcting the Minimization Bias in Searches for Small Signals*," *arXiv: hep/ph*, vol. 0206139, 2002.

[9] R. Cousins and V. Highland, "*Incorporating Systematic Uncertainties into an Upper Limit*," *Nucl: Inst. and Meth. in Physics Research A*, vol. 320, p. 331, 1992.